4-22-96

SANDIA REPORT

SAND95–1240 • UC–721
Unlimited Release
Printed April 1996

Petrographic and X-Ray Diffraction Analyses of Selected Samples from Marker Bed 139 at the Waste Isolation Pilot Plant

Joanne T. Fredrich, David H. Zeuch

Prepared by
Sandia National Laboratories
Albuquerque, New Mexico 87185 and Livermore, California 94550
for the United States Department of Energy
under Contract DE-AC04-94AL85000

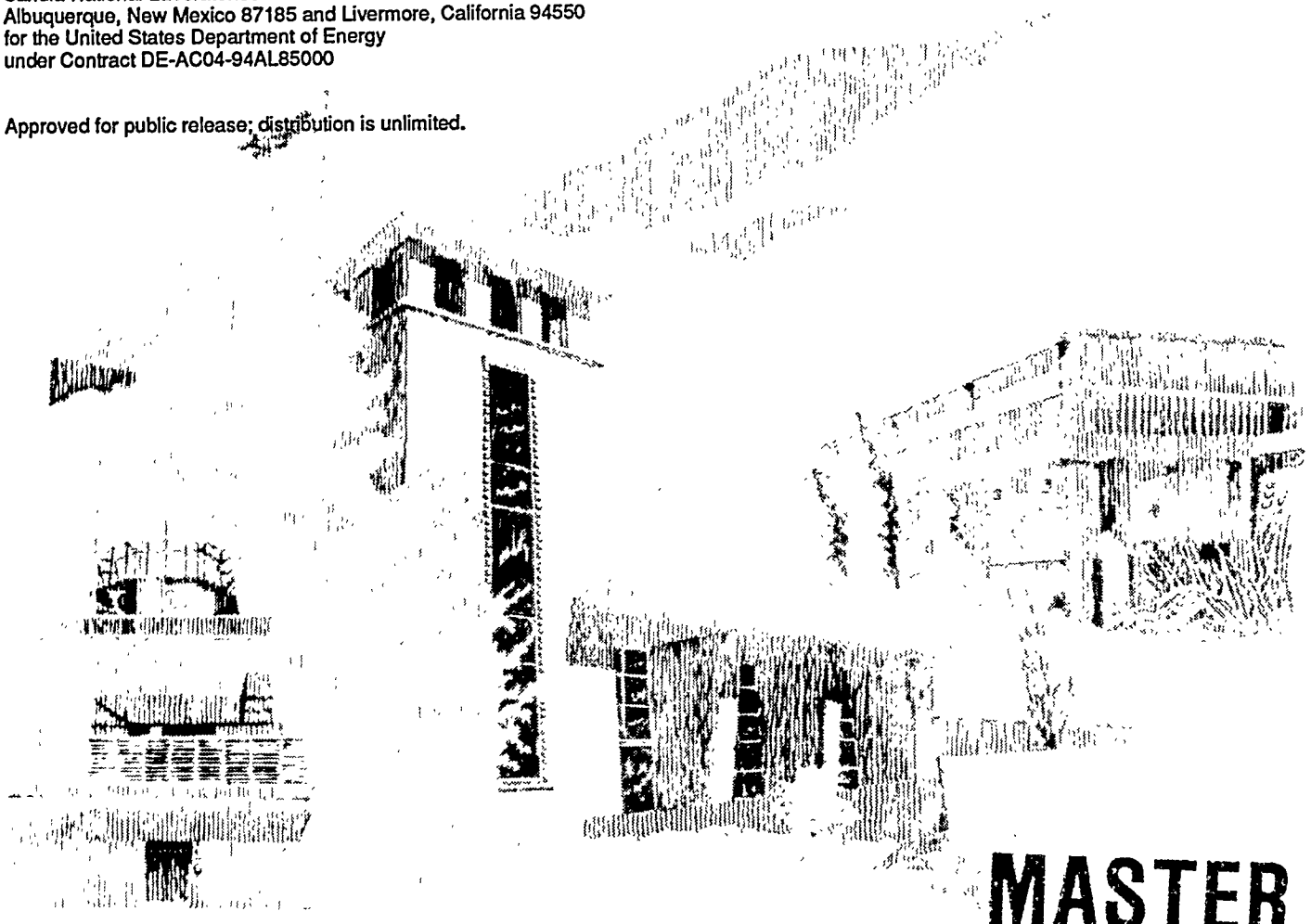

Issued by Sandia National Laboratories, operated for the United States Department of Energy by Sandia Corporation.

Available to DOE and DOE contractors from
Office of Scientific and Technical Information
PO Box 62
Oak Ridge, TN 37831

Prices available from (615) 576-8401, FTS 626-8401

Available to the public from
National Technical Information Service
US Department of Commerce
5285 Port Royal Rd
Springfield, VA 22161

NTIS price codes
Printed copy: A04
Microfiche copy: A01

SAND95-1240
Unlimited Release
Printed April 1996

Distribution
Category UC-721

Petrographic and X-Ray Diffraction Analyses of Selected Samples from Marker Bed 139 at the Waste Isolation Pilot Plant

Joanne T. Fredrich and David H. Zeuch
Geomechanics Department 6117
Sandia National Laboratories
Albuquerque, NM 87185-0751

ABSTRACT

This report synthesizes petrographic and x-ray powder diffraction studies performed on Marker Bed 139 core samples to support the Salado Two-Phase Flow Laboratory Program. Experimental scoping activities were performed in FY 1993 by three independent commercial laboratories in order to quantify the mineral composition to complement laboratory studies of hydrologic properties and to describe textures and porosity. Samples from various depth intervals were prepared from six 6-inch diameter cores which were obtained by drilling into the marker bed from the floors of the E140 drift and Room 3. The petrographic analyses were augmented here by additional study of the original thin sections. Also, the pore structure observations are examined in relation to independent observations of microcracks in Marker Bed 139 core samples performed for the Core Damage Assessment Study of the Salado Two-Phase Flow Laboratory program in FY 1994 by the Geomechanics Department. Some revisions to Borns's (1985) earlier mesoscopic mineralogic/textural classification of the marker bed into five zones are proposed in light of the more detailed quantitative laboratory analyses and petrographic studies. The detailed studies reveal that heterogeneity persists at even the centimeter scale within individual zones of the marker bed. The major phases in the marker bed are anhydrite, halite, and polyhalite. However, the most commonly observed form of porosity is a penetrative microporosity that is consistently associated with a minor-phase, finely crystalline carbonate that occurs both in isolated patches and in fine laminations or "stringers." Other observed porosity occurs in the form of discrete microfractures which are sometimes closely associated with the carbonate "stringers." The "stringers" may represent relict surfaces of fluid transport and dissolution and be persistent planes of weakness within the marker bed. The origin of many of the observed microfractures is unclear; however, the presence of partially and fully mineralized microcracks indicates that at least some of these microfractures are open in the marker bed as it exists *in situ*.

TABLE OF CONTENTS

LIST OF FIGURES

LIST OF TABLES

1.0 INTRODUCTION

1.1 Background and Rationale

The Waste Isolation Pilot Plant (WIPP) is the U.S. Department of Energy's planned repository for transuranic waste generated by defense programs. The WIPP repository is located 660 m underground in the Salado Formation, which consists of thick, horizontally bedded pure and impure salt and thin, laterally continuous clay and anhydrite interbeds. Forty-five numbered marker beds (from Marker Bed 100 to Marker Bed 144) are identified in the formation. Marker Beds 138 and 139 and anhydrites "a" and "b" are located in the immediate vicinity of the repository horizon.

Over a long time period, anoxic corrosion and microbial degradation of contact-handled transuranic waste may produce sufficient quantities of gas to generate high pressures in the disposal rooms at the WIPP repository (Davies, 1991). Field measurements indicate that the permeability of the nonhalite interbeds may be one to four orders of magnitude higher than that of the pure and impure halite beds (Davies et al., 1991; Beauheim et al., 1993a). Owing to a combination of their higher intrinsic permeability and estimated lower threshold pressure, the interbeds are expected to be the dominant pathways for the flow of waste-generated gas away from the pressurized repository (Davies, 1991).

The Salado Two-Phase Flow Laboratory Program was established to provide site-specific two-phase flow and other related rock properties to support performance assessment modeling of the WIPP repository (Howarth, 1993; 1994). Owing to their potentially significant role in the hydrologic response of the repository, the program initially focused on the anhydrite interbeds, and in particular, on Marker Bed 139 (MB 139), which lies approximately 1 m below the planned waste storage rooms (Figure 1).

This report synthesizes petrographic and x-ray powder diffraction studies performed to support the Salado Two-Phase Flow Laboratory Program (Howarth, 1993). Experimental scoping activities in this area were performed in FY 1993 by three independent laboratories in order to: (1) quantify the mineral composition to support laboratory studies of hydrologic properties and facilitate correlation of transport properties with composition; (2) describe textures, including grain size; and (3) describe observed porosity. Samples from various depths were prepared from six 6-inch diameter cores which were obtained by drilling into the marker bed from the floor of two separate rooms. The petrographic analyses are augmented here with additional study of the original thin sections, and the pore structure observations are also examined in relation to an independent observational study of microcracks in Marker Bed 139 core samples performed in FY 1994 by the Geomechanics Department at Sandia National Laboratories.

1.2 Geologic Overview of Marker Bed 139

Borns (1985) discusses the paleoenvironment in which the Salado Formation was deposited and provides a mesoscopic description of MB 139 based on study of whole and slabbed cores obtained from a five-hole array drilled into the marker bed from the floor of Room 4. To summarize, Borns (1985) sees MB 139 as representing a period of intermittently shallow water deposition in the cyclic flooding-desiccation sequence which characterizes the transitional paleoenvironment (from marine and reefoid limestones to redbeds) in which the Salado was deposited (e.g., Lowenstein, 1982). The primary evidence for this conclusion comes from growth structures exhibited by halite in the marker bed, including swallowtail structures and hopper crystals. Borns (1985) further interprets halite replacing anhydrite groundmass and halite pseudomorphs exhibiting primary gypsum growth structures (swallowtail structures) as evidence for postdepositional diagenetic alterations.

Based upon his mesoscopic examination, Borns (1985) proposed that MB139 could be divided into five stratigraphically distinct zones: upper and lower contact zones marked by conspicuous clay layers (I and V), a massive polyhalitic anhydrite zone (II), a mixed anhydrite/polyhalitic anhydrite zone (III), and a laminated anhydrite with halite zone (IV). Recent *in situ* hydrofracture tests suggest that partially or fully healed fractures in the bottom third of the marker bed are the dominant flow paths (Beauheim et al., 1993b).

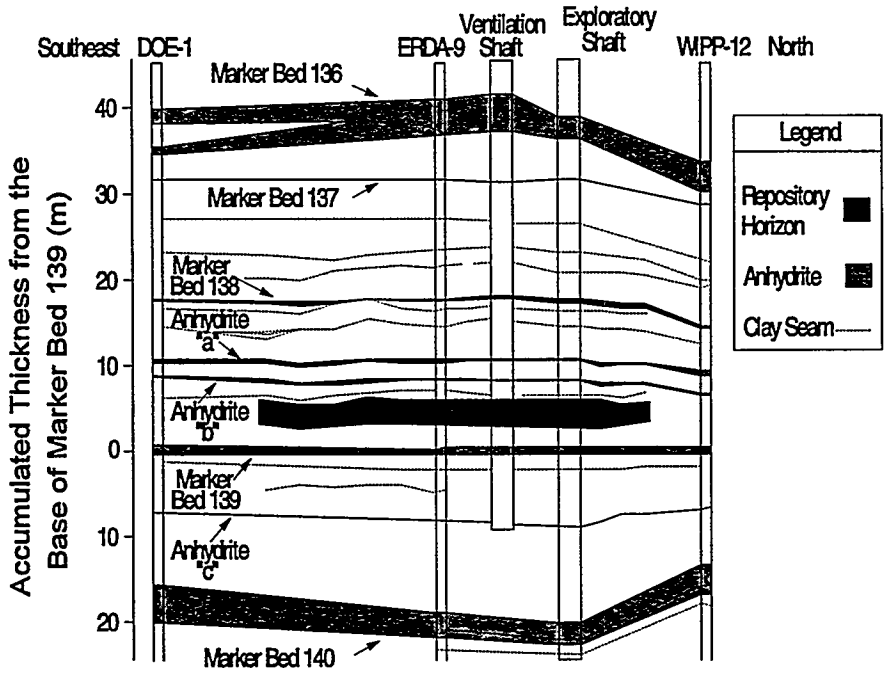

Figure 1. Local stratigraphic sections directly above and below the repository horizon (modified from Davies et al., 1991).

2.0 CORE SAMPLES AND METHODS OF STUDY

2.1 Marker Bed 139 Samples

2.1.1 Borehole Locations and Core Retrieval

Laboratory analyses were performed on cores obtained from holes drilled vertically into the floor from Room 3 and at the E140 drift just north of the N1100 drift (Table 1 and Figure 2). The cores were drilled with air and were nominally 6 inches in diameter.

Table 1. Borehole Data for MB 139 Cores

Borehole No.	Coordinate N* (feet)	Coordinate E† (feet)	Room	Elevation at collar‡ (feet)	Drilling date
E1X07	10830.61	7064.48	E140	1302.46	11/12/92
E1X08	10998.45	7064.97	E140	1303.09	11/12/92
E1X10	10992.22	7064.8	E140	1303.12	11/16/92
E1X11	10988.49	7065.02	E140	1303.14	11/16/92
P3X10	11103.34	6385.3	3	1297.27	4/27/92
P3X11	11101.62	6385.46	3	1297.26	4/28/92

* To convert this coordinate to the WIPP coordinate system (Gonzales, 1989), add 490,000.00 to the coordinate value given here.

† To convert this coordinate to the WIPP coordinate system (Gonzales, 1989), add 660,000.00 to the coordinate value given here.

‡ Relative to mean sea level.

Room E140 was excavated in April of 1983, whereas Room 3 dates back to February of 1983. Thus, any changes in the *in situ* pore structure related to the formation of a disturbed rock zone around an underground excavation (Borns and Stormont, 1989) are expected to be nominally identical since the MB 139 cores were all drilled ~9.2-9.6 years after excavation.

2.1.2 Sampling Strategies for Laboratory Tests

Three independent laboratories performed x-ray powder diffraction (XRD) and petrographic analyses on samples taken from several depth intervals for each of the cores as described in Table 2. The depth intervals which were sampled are detailed in Tables 3 and 4. Note that the intervals are relative to the elevation at the borehole collar (Table 1).

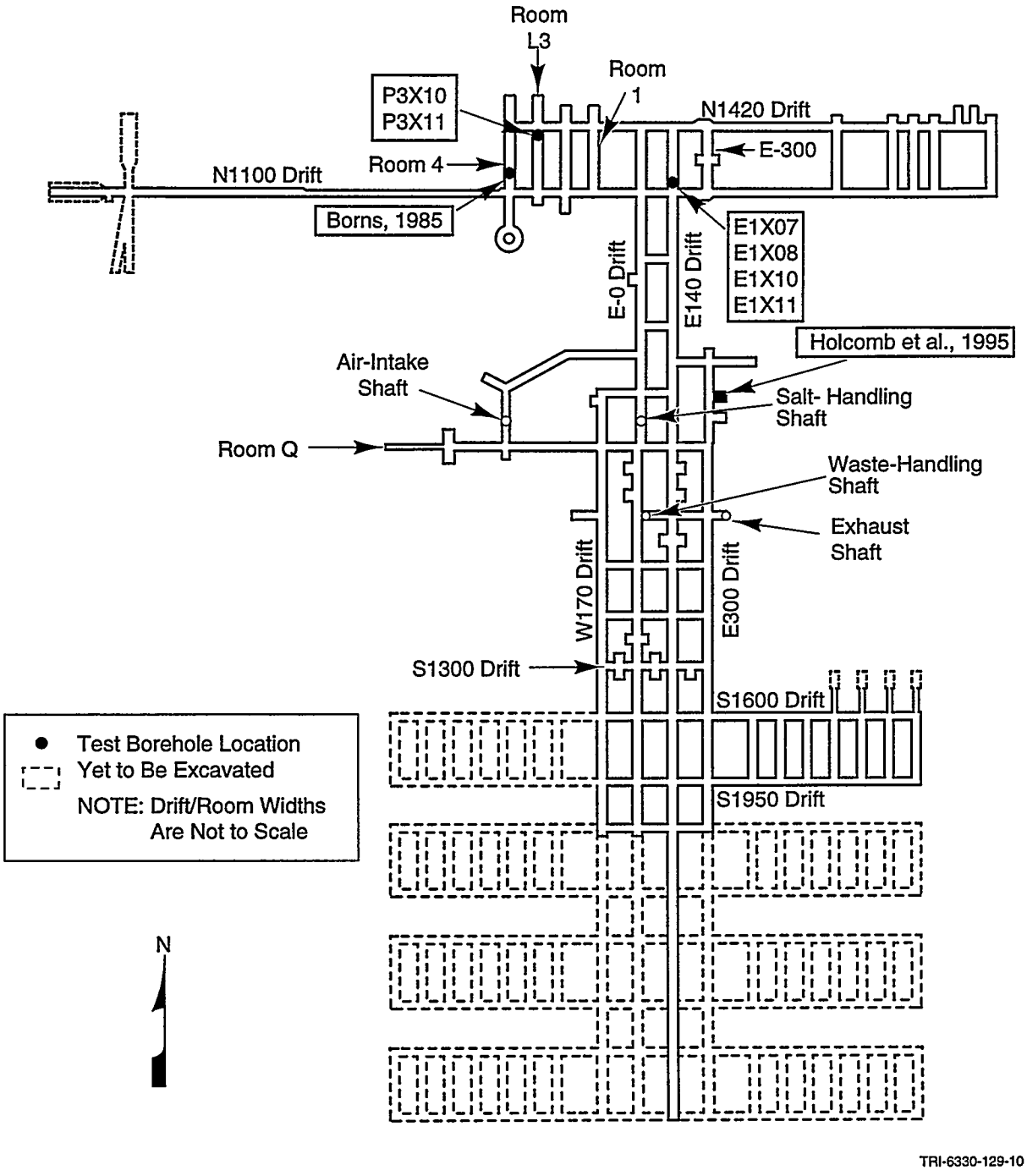

Figure 2. Configuration of the underground facility showing location of MB 139 core samples taken for this study. For reference, the locations of the MB 139 core samples previously studied by Borns (1985) and Holcomb et al. (1995) are also shown.

Table 2. Test Matrix for MB139 Cores

Core I.D.	Number of intervals sampled for XRD analyses	Contractor for XRD analyses	Number of intervals sampled for petrographic analyses	Contractor for petrographic analyses
E1X07	3	University of Utah Research Institute, Salt Lake City*	3†	TerraTek, Inc. Salt Lake City, UT
E1X08	3	University of Utah Research Institute, Salt Lake City*	3†	TerraTek, Inc. Salt Lake City, UT
E1X10	6‡	Omni Laboratories, Inc., Houston, TX**	6‡	Omni Laboratories, Inc., Houston, TX**
E1X11	5‡	Omni Laboratories, Inc., Houston, TX**	5‡	Omni Laboratories, Inc., Houston, TX**
P3X10	2§	South Dakota School of Mines and Technology, Rapid City***	1†	South Dakota School of Mines and Technology, Rapid City***
P3X11	4¶	South Dakota School of Mines and Technology, Rapid City***	2†	South Dakota School of Mines and Technology, Rapid City***

* Subcontracted by TerraTek, Inc., Salt Lake City, Utah.
** Subcontracted by Rock Physics Associates, San Jose, California.
*** Subcontracted by RE/SPEC, Rapid City, South Dakota.
† Three mutually perpendicular thin sections were prepared from each depth interval.
‡ For two of the depth intervals, one analysis each was performed on a sample prepared parallel and perpendicular to bedding.
§ For one of the depth intervals, analyses were performed on two samples obtained from the same depth interval but spaced ~4 inches apart horizontally (in the bedding plane).
¶ For two of the depth intervals, analyses were performed on two samples obtained from the same depth interval but spaced ~4 inches apart horizontally (in the bedding plane).

Table 3. Core Depths Sampled for XRD Analyses

Core i.d.	Depth interval (feet)	No. of samples	Contractor sample i.d.
E1X07	4.00-4.14	1	PX4
	5.00-5.14	1	PX5
	5.73-5.87	1	PX6
E1X08	4.00-4.14	1	PX1
	4.86-5.00	1	PX2
	5.71-5.85	1	PX3
E1X10	4.50*	1	01
	5.00*	1	02
	5.25*	2	03, 04
	5.50*	1	05
	5.75*	2	06, 07
	6.25*	1	08
E1X11	4.50*	1	09
	4.75*	1	10
	5.00*	1	11
	5.25*	2	12, 13
	5.75*	2	14, 15
P3X10	5.15-5.39	1	P3X10-5-3-2-TS2-4
	5.53-5.87	2	P3X10-6-SP2T, P3X10-6-SP2B
P3X11	5.33-5.67	2	P3X11-5-2-SP1T, P3X11-5-2-SP1B
	5.84-6.04	1	P3X11-5-2-TS1-4
	6.88-7.22	2	P3X11-5-3-SP3T, P3X11-5-3-SP3B
	7.55-7.72	1	P3X11-6-TS3-4

* The exact depth interval used for sample preparation was not recorded.

Table 4. Core Depths Sampled for Petrographic Analyses

Core i.d.	Depth interval (feet)	No. of samples	Contractor sample i.d.
E1X07	4.00-4.14	3*†	PX4-O1, PX4-O2, PX4-O3
	5.05-5.14	3*†	PX5-O1, PX5-O2, PX5-O3
	5.73-5.87	3*†	PX6-O1, PX6-O2, PX6-O3
E1X08	4.00-4.14	3*†	PX1-O1, PX1-O2, PX1-O3
	4.86-5.00	3*†	PX2-O1, PX2-O2, PX2-O3
	5.71-5.85	3*†	PX3-O1, PX3-O2, PX3-O3
E1X10	4.50**	1‡	01 (H-4.50')
	5.00**	1‡	02 (H-5.00')
	5.25**	2‡§	03, 04 (V-5.25', H-5.25')
	5.50**	1‡	05 (H-5.50')
	5.75**	2‡§	06, 07 (V-5.75', H-5.75')
	6.25**	1§	08 (V-6.25')
E1X11	4.50**	1‡	09 (H-4.50')
	4.75**	1‡	10 (H-4.75')
	5.00**	1‡	11 (H-5.00')
	5.25**	2‡§	12, 13 (V-5.25', H-5.25')
	5.75**	2‡§	14, 15 (V-5.75', H-5.75')
P3X10	5.15 5.18-5.39	3*	P3X10-5-3-2-TS2-1 P3X10-5-3-2-TS2-2 , P3X10-5-3-2-TS2-3
P3X11	5.80 5.84-6.04	3*	P3X11-5-2-TS1-1 P3X11-5-2-TS1-2 , P3X11-5-2-TS1-3
	7.55 7.55-7.72	3*	P3X11-6-TS3-1, P3X11-6-TS3-2 , P3X11-6-TS3-3

* One section was oriented parallel to bedding whereas the other two were vertical and mutually perpendicular.
** The exact depth interval used for sample preparation was not recorded.
† The section oriented parallel to bedding was prepared from the middle of the given depth interval.
‡ Section was oriented vertically (perpendicular to bedding).
§ Section was oriented horizontally (parallel to bedding).

2.2 Procedures

2.2.1 Thin Section Preparation

Polished thin sections with a thickness of ~30 μm were prepared from each of the core samples using standard abrasive polishing techniques. The samples from cores E1X07, E1X08, E1X10, and E1X11 were vacuum impregnated with an epoxy containing a blue dye prior to thin section preparation; however, the samples from cores P3X10 and P3X11 were not. The thin sections prepared from cores E1X07 and E1X08 were oversized (nominal glass slide dimensions of 2×3 inches compared with the conventional 1×1.8 inches). Three mutually perpendicular samples were prepared from each of the locations sampled from cores E1X07, E1X08, P3X10, and P3X11; however, only one or two orientations were prepared from each of the locations sampled from cores E1X10 and E1X11. Finally, it appeared that chips, rather than intact samples, were used for thin section preparation from cores E1X10 and E1X11.

2.2.2 Petrography

Petrography was conducted using a polarizing optical microscope and both plane-polarized and cross-polarized light. Minerals were identified using standard petrographic techniques, including appearance, extinction, birefringence, cleavage, crystal habit, pleochroism, and interference, and following reference texts (e.g., Deer et al., 1966; Adams et al., 1984; Kerr, 1977).

2.2.3 X-Ray Diffraction

X-ray powder diffraction (XRD) is an analytical technique for semiquantitative analysis of mineral components, including those too fine grained to be identified using light microscopy techniques. An x-ray beam is projected onto a powdered sample and the angles at which specific characteristic wavelengths are diffracted are measured. The complete diffraction pattern is analyzed to identify mineralogy and approximate abundance. The procedures used by the different laboratories for the so-called "bulk" analyses that were performed for this effort varied somewhat and are summarized in Table 5.

Variables that can affect calculation of the proportion of each mineral phase in a sample include peak overlap, crystallinity and crystal size, amorphous or organic content, absorption factors, chemical substitution, matrix absorption, preparation techniques, and detection limits. Although many of these variables can be controlled, some cannot; hence, the results of XRD analyses are only semi-quantitative. Typical errors are up to ±10% of the amounts present for major phases (≥20% bulk composition) and up to ±20% for minerals present in concentrations less than this (Moore and Reynolds, 1989).

Table 5. Procedures Used for X-Ray Powder Diffraction

Core i.d.	Size Fraction	Scan Interval	Technique	Reference
E1X07, E1X08	≤45 μm	2-65°2θ	Reference Intensity Ratio (RIR)†	Jenkins (1986)
E1X10, E1X11	15 μm*	2-70°2θ	RIR‡	Chung (1974)
P3X10, P3X11	< 10 μm	3-60°2θ	RIR	Chung (1974)

* Typically, 80% falls within 12-18 μm particle size.
† Average of three duplicate samples.
‡ Average of six duplicate runs (occasionally, results of disparate runs were not included).

2.2.4 Modal Analysis and Grain Size Distribution

Each thin section was examined under a polarizing optical microscope and either 180- or 300-point counts were performed to determine bulk composition. For two sets of the thin sections (E1X07 and E1X08), the maximum grain dimension was measured simultaneously with an eyepiece micrometer.

This page intentionally left blank.

3.0 PETROGRAPHY

As noted in Section 2.2.1, three mutually perpendicular thin sections were prepared from each location sampled for cores E1X07, E1X08, P3X10, and P3X11 (one section oriented nominally parallel to bedding and two mutually perpendicular sections oriented perpendicular to bedding), whereas only one or two sections were prepared from each of the locations sampled from cores E1X10 and E1X11 (Table 4). The E1X07, E1X08, P3X10, and P3X11 sections also provided significantly greater continuous surface area for examination than did the E1X10 and E1X11 sections. The textural observations are thus derived principally from the former sections, although they were compared against the latter sections for consistency. In addition, of the E1X07, E1X08, P3X10, and P3X11 sections, only those prepared from cores E1X07 and E1X08 were impregnated with a dyed epoxy prior to sectioning. Thus, the porosity observations are based primarily on the sections prepared from cores E1X07 and E1X08, although they were again compared with sections prepared from cores P3X10, P3X11, E1X10, and E1X11 for consistency.

3.1 Textures and Diagenetic Features

3.1.1 Overview

The principal mineral constituents of MB139 are anhydrite, halite, and polyhalite, although minor quantities of finely crystalline carbonate are present, as are trace amounts of clay and bituminous material. Distribution of the three dominant minerals is highly variable both vertically and laterally, even on the centimeter scale of the standard petrographic thin section. Textures are similarly varied. Textural and mineralogical differences are even greater between boreholes, where some mineralogic zones may be altogether absent. Paradoxically, inhomogeneity may thus be one of the most characteristic features of MB139.

A comprehensive microscopic investigation of the diagenetic and geologic history of the marker bed is beyond the scope of this report, which instead focuses on the salient features (both similarities and differences) of the sections that were examined, relating them to the mesoscopically identified zones of Borns (1985) where possible. Although it is possible that future microscopic observations of new cores drilled into the marker bed may reveal additional features, the following petrographic observations derived from three different sets of boreholes are believed to capture many of the areally consistent features of the marker bed.

3.1.2 Polyhalite

The presence of polyhalite is the defining feature of Borns's (1985) mesoscopically identified Zone II, which he considered to comprise approximately the upper third of MB 139. Polyhalite is generally absent in Zones III and IV. Consistent with this classification, polyhalite was only observed in samples taken from the uppermost portion of the marker bed. Although polyhalite predominates in

several sections (e.g., PX1-01 and PX1-03), it may grade abruptly into anhydrite and halite, and disappear almost completely over only a few centimeters (PX1-02). Polyhalite is entirely absent in any of the sections prepared from boreholes E1X10 and E1X11.

Polyhalite occurs as fine, feathery, or acicular crystals which form pinkish, spherulitic, pseudocrosslike or radial structures. Where polyhalite dominates, the spherulitic structure is most prominent (Figure 3a). The spherules consist of fine-grained polyhalite crystals which may exhibit a radial structure (e.g., PX1-01) or, alternatively, appear randomly oriented (e.g., P3X11-5-2-TS1-2). The spherules are intergrown to form a dense, tightly interlocked crystal mass with fine-grained halite, anhydrite, and carbonate filling spaces between spherulites. The outer margins of the individual spherules may be darkened by finely crystalline carbonate, resulting in a mottled, pseudo-orbicular texture.

Where polyhalite and anhydrite are present in more equal proportions, the spherulitic habit again dominates. The spherules may appear as isolated features scattered in finely crystalline anhydrite (e.g., P3X11-5-2-TS1-1 and P3X11-5-2-TS1-3), or massed together in thin laminae (P3X11-5-2-TS1-2) subparallel to bedding. There is a weak tendency for the spherules to be elongated subparallel to bedding in this last section. The polyhalitic laminae appear to flow around and fill spaces in between lenses of massive anhydrite. The concentration of polyhalite in more-or-less distinct laminations in samples from core P3X11 differs markedly from the more massive habit characteristic in samples from cores E1X07 and E1X08.

With increasing halite content, the radial and pseudocrosslike structures are more common, particularly when the two minerals are in direct contact (Figure 3b). These structures are characterized by longer, more slender needlelike crystals than those typical of the spherulitic structure.

3.1.3 Anhydrite

In Borns's (1985) classification, anhydrite occurred in Zones II, III, and IV, and increased with depth to become a dominant mineral in Zone IV. Anhydrite is commonly finely crystalline, untwined, and ranges in shape from euhedral to anhedral. In association with polyhalite (i.e., in the uppermost portion of the marker bed), it appears as isolated, euhedral to subhedral elongated laths and equant tablets (Figure 3a), and as finely crystalline infilling between intergrown spherules. With increasing depth in the marker bed, polyhalite first diminishes, then disappears, whereas halite content increases and comprises up to half of the rock. Anhydrite then appears as finely crystalline, homogeneous, randomly oriented masses that surround larger, isolated grains of halite. At the margins of halite grains, however, anhydrite grain size may abruptly increase and grain shapes become euhedral. Similarly, grain size can vary abruptly in the massive anhydrite zones, with lenses of relatively coarse-grained anhydrite surrounded by fine-grained material. Except for this dramatic difference in grain size relative to the surrounding mass (an order of magnitude or greater), these lenses or pods are otherwise structureless.

In some areas, anhydrite forms concentric polygonal structures (Figure 4), alternating repeatedly with single-crystal halite (e.g., PX5-05). These structures can be large and prominent, up to 0.5 cm in diameter. The anhydrite crystals grow as fine tablets or laths normal to the polygon walls, and both into and out of the polygons; a distinct median line separates those grains growing into and out of the polygons, resulting in a sort of "bidentate" appearance. While complete polygons are rare, fragments of polygon walls are common both within anhydrite masses and as salients in large halite grains. This structure indicates that both anhydrite and halite are pseudomorphous after gypsum, which was almost certainly the original sulfate mineral precipitated from solution (Blatt et al., 1972). (Subsequently, upon burial and dewatering, the primary gypsum is replaced by anhydrite and halite.) The "fragmentary" remains of the pseudomorphs suggest that early transformation of gypsum to anhydrite may have been accompanied or followed by local deformation and additional replacement.

With yet greater depth, the amount of halite diminishes and anhydrite becomes the dominant mineral. Halite is absent in several of the sections taken from the greatest depths of cores E1X10 and E1X11 (V-5.75' and V-6.25'), and largely absent in sections taken from the greatest depth in core P3X11 (P3X11-6-TS3-1 and P3X11-6-TS3-2). Texturally, however, the anhydrite is identical to that of the relatively homogeneous massive anhydrite higher up in the marker bed, except that the expanses uninterrupted by halite are more extensive areally.

3.1.4 Halite

Halite is present in at least some of the sections prepared from each depth for all cores. It is almost always much coarser-grained than polyhalite and anhydrite, ranging from 0.1 to 3 cm in diameter. Halite usually occurs as large, anhedral, isolated single crystals surrounded by polyhalite and/or anhydrite. Shapes are extremely irregular, often convoluted. Particularly when in contact with anhydrite, grain boundaries are ragged and vague. Long salients of polycrystalline anhydrite (and, when present, polyhalite needles) often extend deeply into halite grains, further enhancing the contorted appearance. Where halite is present in the greatest quantities, the net effect is a distinctive patchy or mottled texture.

Grains are filled with inclusions in varying degrees, resulting in an overall dusty or dirty appearance. While many grains are generally or partially free of inclusions, others are so filled with patches of single- and polycrystalline anhydrite that the minerals are present in roughly equal amounts, suggesting a replacement texture. Other inclusions consist of finely crystalline carbonate patches, possibly clays and bituminous material, and fluids. Fluid inclusions occur in isolation, or in planar and curviplanar arrays (Figure 5). Cleavage planes are often decorated with finely crystalline carbonate or bitumen, possibly suggesting that they were once fractured. Both the fluid inclusion arrays and decorated cleavage planes may be healed fractures whose possible origins are remarked upon later.

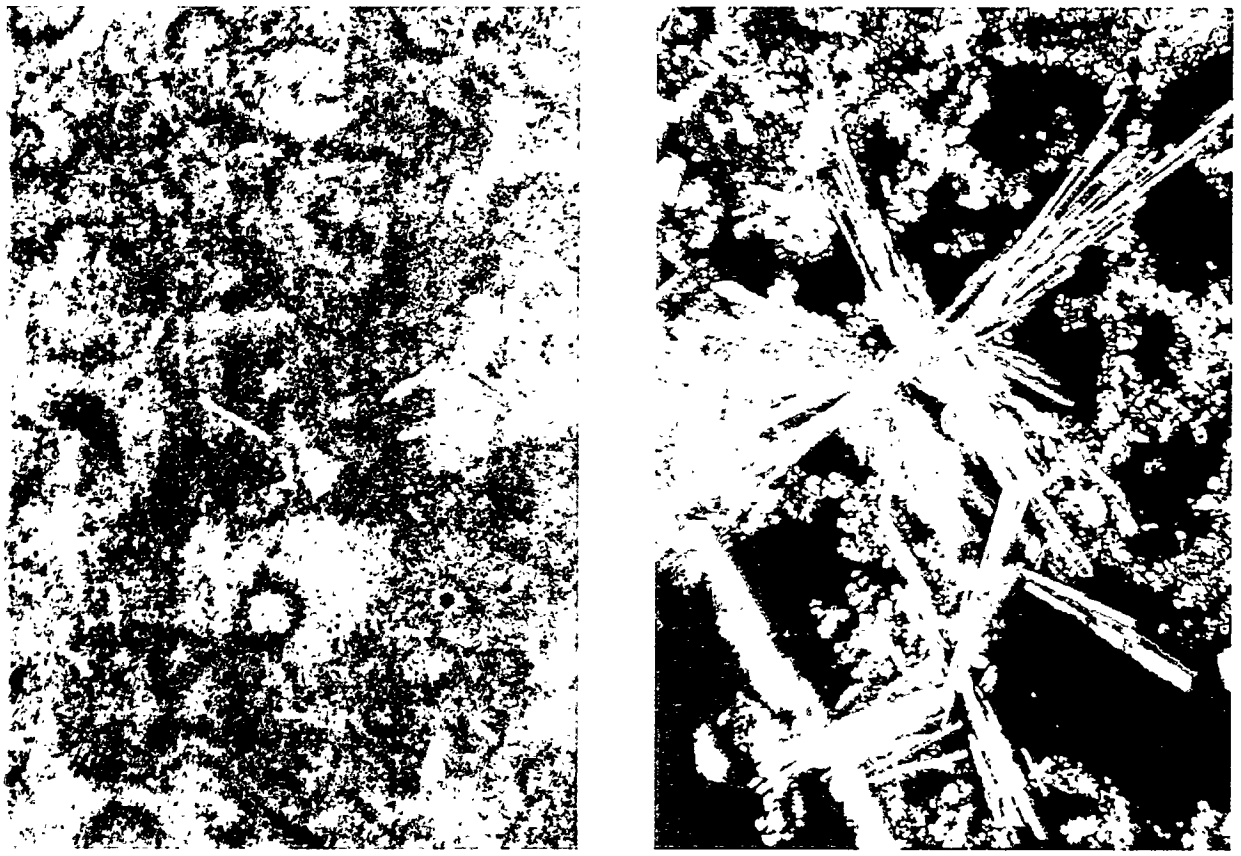

(a) (b)

Figure 3. (a) Spherulitic texture of polyhalite. Dark carbonate and clay minerals concentrate at the margins of the salmon-pink spherulites, creating a pseudo-orbicular texture. Note the long, isolated laths of anhydrite. Width of field is 2.23 mm. Plane polarized light. (b) Pseudo-cross and radial habits of polyhalite (long needles) when halite (black regions) is present in large quantities. Width of field is 2.23 mm. Crossed polarizers.

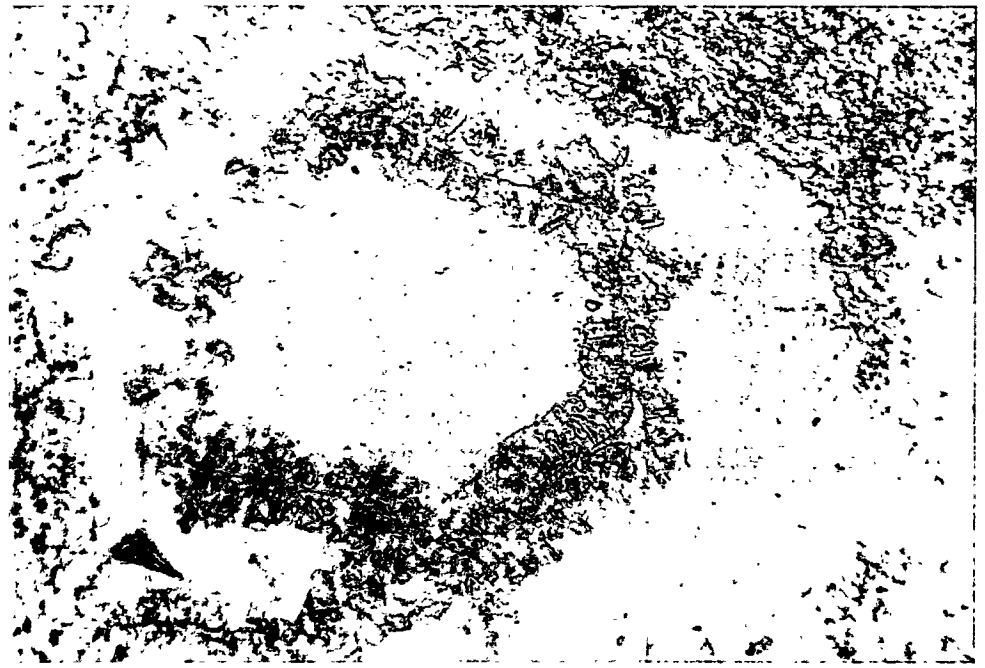

(a)

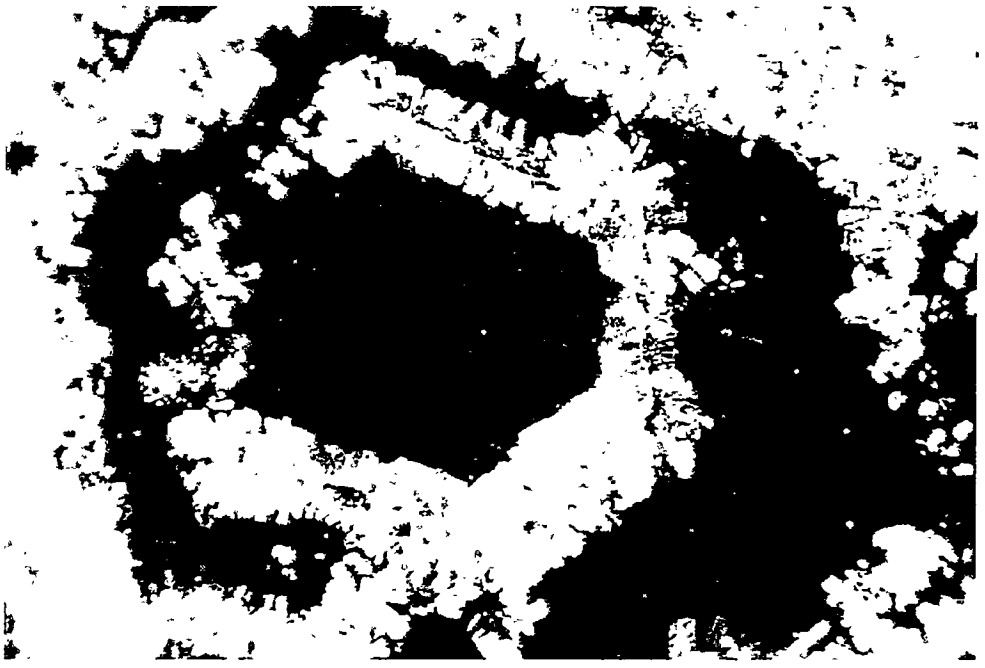

(b)

Figure 4. (a) Polygonal anhydrite-halite pseudomorph after gypsum. Width of field is 3.45 mm. Plane polarized light. (b) Same area, crossed polarizers. Anhydrite is finely crystalline and highly birefringent; halite appears black.

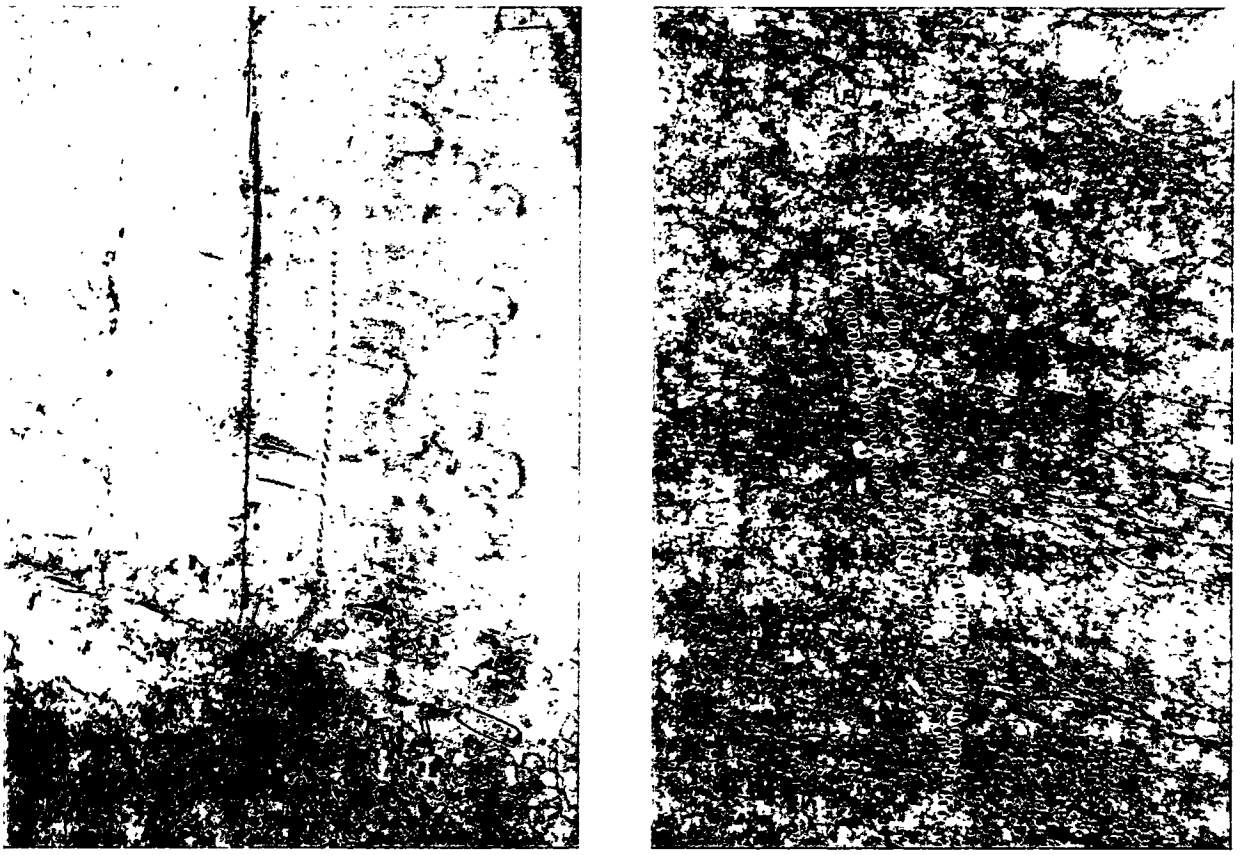

(a) (b)

Figure 5. (a) Planar arrays of fluid inclusions in halite which probably represent healed microfractures. Width of field is 2.23 mm. Plane polarized light. (b) Healed fracture in finely crystalline anhydrite. The fracture is filled primarily with anhydrite, but a very narrow aperture is present at the center (edges dotted for clarity). Width of field is 2.23 mm. Plane polarized light.

3.1.5 Carbonates and Clays

Although carbonate and clay minerals are present in only minor amounts throughout the marker bed, their mode of occurrence is an important aspect of the mesoscopic and microscopic structure of MB 139. In particular, they are closely associated with both the little native porosity which exists in the marker bed and with the development of excavation- and coring-induced porosity.

Finely crystalline carbonate (<10 microns) appears as small, discrete, gray-to-brown or semiopaque-to-opaque patches, occasionally as inclusions in halite grains, and also in thin, discontinuous, diffuse stringers oriented subparallel to bedding. As discussed later, carbonates are closely associated with the little porosity which is observed in thin section. The stringers also contain clay minerals, and, possibly bituminous material. Where stringers are present, they commonly separate regions differing in texture and/or composition (e.g., pure anhydrite from patchy halite and anhydrite, or pure anhydrite from mixed anhydrite and polyhalite, or relatively "clean" anhydrite from "dirty"anhydrite).

The stringers, which are undulose and sometimes highly contorted, are most common and areally persistent in sections taken from the greatest depths of cores E1X07, E1X08, P3X10, and P3X11, resulting in a mesoscopically laminated appearance. When stringers curve around halite lenses, the boudinagelike appearance of halite lenses is enhanced (e.g., PX6-02 and PX3-02). Although less common in the uppermost, polyhalitic intervals, bedding-plane stringers are still occasionally prominent (e.g., PX1-02, P3X11-5-2-TS1-2, and P3X11-5-2-TS1-3). They are least common and extensive in the middle depth.

The stylolytic appearance of the stringers suggests that they may represent relict surfaces of fluid transport and dissolution (Lowenstein, 1982; Borns, 1985); the relatively insoluble opaques may have been concentrated and left behind as fluids were driven off first by burial and then by dewatering of gypsum. Their convoluted character might be attributable to local deformation associated with the dehydration reaction and related either to the large volume change associated with gypsum→aragonite reaction or else to the development of high pore pressures (Blatt et al., 1972; p. 505). The development and healing of microfractures in halite discussed previously may also be related to this latter aspect.

3.2 Porosity Description

3.2.1 Overview

Although there has been at least one earlier episode of fracturing and rehealing in Marker Bed 139 prior to core recovery, detailed investigation of this history is beyond the scope of this report. This study focuses on the occurrence of open and interconnected porosity in the marker bed, as identified by its penetration by dyed epoxy. Interconnected porosity is the primary concern for estimating the hydrological transport properties of the marker bed, whereas the healed paleomicrofractures are of secondary interest.

Porosity is most consistently associated with the finely crystalline carbonate which occurs in patches and stringers. Most often, the porosity occurs as a penetrative microporosity throughout many of the carbonate patches. The only other observed porosity is in the form of discrete microfractures, some of which are again closely associated with the carbonate stringers. Examination at high magnifications revealed no detectable population of microfractures or other porosity not penetrated by the dyed epoxy. None of the sections contained a high density of microfractures.

Some of the observed healed microfractures almost certainly date back to early diagenesis, including burial, compaction, and gypsum dehydration. The planar fluid inclusion arrays, which possibly mark healed fractures, may date back to this early diagenetic stage. The observed small, isolated now-sealed fractures in the massive anhydrite (Figure 6) and the longer, stylolytic stringers may mark the site of previously open microfractures. Thus, regarding the long-term stability of the WIPP repository, there is evidence that under some circumstances the marker bed may be capable of "healing" itself. However, there is also evidence that the previously healed microfractures may be preferred sites for the development of excavation- and coring-induced microfracturing, and, hence, persistent planes of weakness in the marker bed.

3.2.2 Microporosity

Whether in isolated patches or discontinuous stringers, the minor carbonate phases are frequently associated with a local porosity greater than that of the surrounding rock. Furthermore, the presence of the blue dye indicates that this porosity is connected within the bulk rock. Often, this microporosity is only revealed by a distinct blue hue overprinting the carbonate patches and stringers, and due to the exceptionally small size of the individual carbonate grains, its detailed character is not readily discernible. This microporosity may be in the form of a fine network of microfractures along grain boundaries of the finely crystalline carbonate (the grain size of which is substantially less than the section thickness), or in the form of an interconnected network of equidimensional voids and/or microfractures between the individual carbonate crystals.

3.2.3 Microfractures

Other occurrences of dye penetration into the bulk rock are limited to discrete microfractures. At least a few open microfractures are present in each section from cores E1X07 and E1X08; however, in some cases the microfractures are restricted to the margins, suggesting that they may have resulted from sample preparation. This is especially true of the polyhalitic sections, which are otherwise unfractured. No unconnected porosity was observed, even at high magnifications.

Microfractures most commonly occur in anhydrite and appear largely intergranular in character. Microfractures in halite are much less common, and tend to be cleavage fractures. Where microfractures cross from an anhydrite grain into a halite grain, the microfracture may make an abrupt change in direction to follow a cleavage direction, and then resume the original trajectory when it

crosses back into anhydrite. Microfractures in anhydrite also sometimes terminate upon intersection with a halite grain. This may result from halite's ability to readily deform by plastic deformation mechanisms (i.e., dislocation glide), which would arrest microfracture propagation.

Microfracture apertures are highly variable, ranging from <1 μm up to 1 mm. Microfractures with measurable openings appear to be restricted to anhydrite masses. Regardless of aperture, however, the individual microfractures appear entirely tensile or extensile in character. There is no detectable shear offset along any of the microfractures, nor is there any evidence of comminuted material within the microfractures. Furthermore, with the exception of the very largest microfractures, all appear to be very well to perfectly mated at the finest scales resolvable. The largest microfractures are very well mated except on the most detailed viewing scale, and so it seems unlikely that any significant shear displacement has occurred along the microfractures.

Microfracture lengths are also highly variable, ranging from a few tens of microns to the full width of the oversized petrographic sections (~6.5 cm). In anhydrite, the longer microfractures are actually narrow, discontinuous fracture zones composed of numerous smaller--but obviously related--microfractures. These zones often resemble ligamentary bridges as presented by Freiman and Swanson (1990; their Fig. 3.3). Ligamentary bridging occurs when remnant islands of unfractured material are left behind, resulting in crack-surface tractions. These tractions tend to shield the macrocrack tip from the full magnitude of the applied stress.

In many of the larger microfractures in anhydrite, whole polycrystalline islands of material are left behind in the midst of the microfractures, surrounded by dyed epoxy, but otherwise undamaged and undeformed. These islands could result from another type of crack-surface traction that can occur, frictional interlocking (Freiman and Swanson, 1990; their Fig. 3.3). This type of traction can result in the growth of branching fractures in a direction opposite to that of the growing macrocrack. If these reverse cracks then reconnect with the main fracture, an "island" is left behind. Although these islands could also result from the linking of bridged cracks, in general they seem more likely to result from frictional interlocking.

As noted earlier, the stringers defined by carbonates and clays appear to be preferential sites for the occurrence of new microfractures (Figure 7). This is most pronounced in sections taken normal to bedding from the greatest depths in cores E1X07 and E1X08 (i.e. PX3-02, PX3-03, PX6-02, and PX6-03). Microfractures faithfully follow undulating stringers for distances of up to several centimeters. Holcomb et al. (in press) reported similar observations.

Many microfractures show evidence of subsequent healing, i.e., partial to complete infilling by halite and/or other minerals (Figures 7, 8). Where infilling by halite has been complete, the margins of the microfractures have been otherwise unaltered: the edges of the microfractures are sharp, lacking gradational selvages or depositional zones. Mating of the two sides of the microfractures is almost perfectly preserved, as are even some of the polycrystalline anhydrite islands that reside within the larger microfractures. It also appears that some of this infilling was fractured again at a later time,

Figure 6. Open fracture (containing blue epoxy) in anhydrite paralleling opaque stringers. Stringers are composed of carbonate and clay minerals, and, possibly, bituminous material. The fracture is partially infilled, and this infilling has been refractured in some areas. Width of field is 2.23 mm. Plane polarized light.

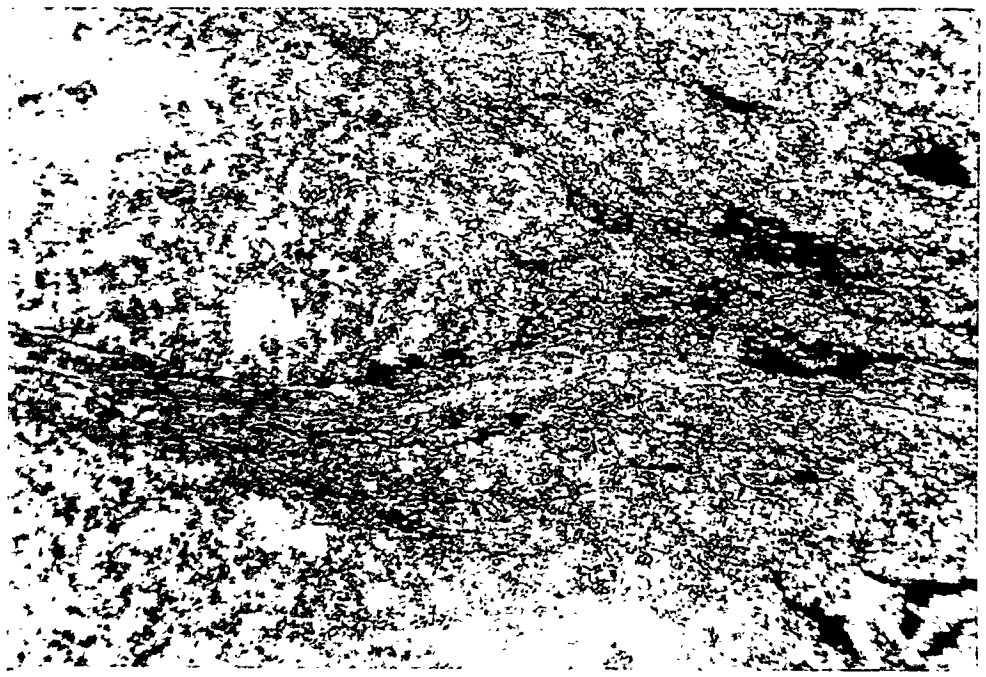

(a)

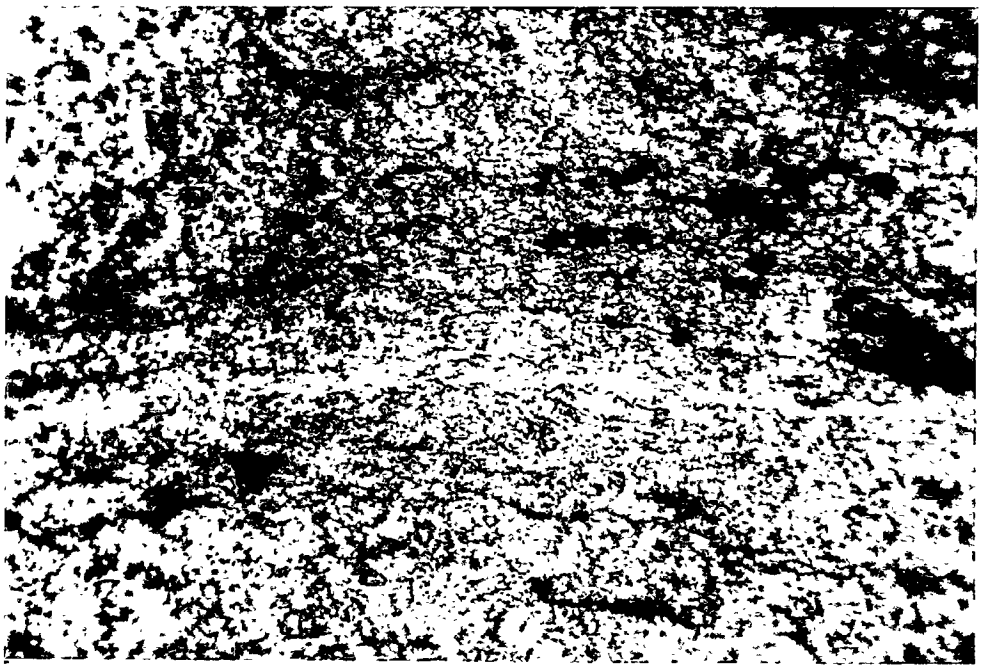

(b)

Figure 7. (a) Partially infilled fracture (containing blue epoxy) in anhydrite. Width of field is 3.45 mm. Plane polarized light. (b) Magnified view, showing blue dye in the interior of the filling, indicating that the filling has been refractured. Width of field is 1.30 mm. Plane polarized light.

(a)

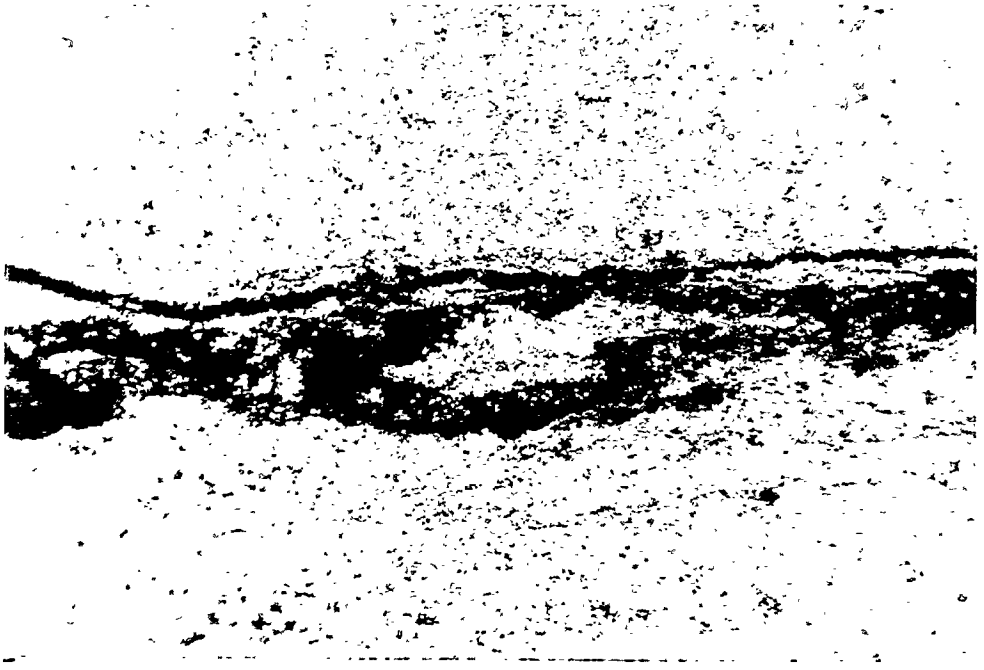

(b)

Figure 8. (a) Wide fracture in anhydrite (speckled brown) that has been filled in completely by halite (tan to white). The fracture contains a small "island" of polycrystalline anhydrite isolated during fracturing. Refracturing of this filled paleofracture (blue epoxy) suggests that it may be a surface of weakness. Width of field is 3.45 mm. Plane polarized light. (b) Same area, crossed polarizers. Halite appears black, anhydrite is finely crystalline and birefringent.

as evidenced by the penetration of the filling by dyed epoxy (Figure 8). The presence and subsequent refracturing of the mineral fillings places some constraints on the timing of fracture development, which is discussed further in the following section.

3.2.3.2 FRACTURE PATTERNS

Owing to the limited and variable microfracturing observed, pattern identification has been done visually. A discernible, repeatable pattern is evident in sections taken from the greatest depths (PX3-02, PX3-03, PX6-02 and PX6-03). The pattern is dominated by a few long microfractures and microfracture zones parallel to subparallel to the trace of bedding, usually following the undulating opaque stringers. Numerous smaller microfractures parallel and subparallel to bedding are also present. It is impossible to estimate a frequency with which these microcracks occur because of the limited sampling; a section may contain as few as one such microcrack or none. Microfractures are concentrated in the massive anhydrite, avoiding the large halite lenses that occur in some of the sections (e.g., PX6-02). A subordinate population of microfractures oriented vertically to bedding is present, some of which are up to 2 cm in length (PX6-01). Microfractures in other orientations (i.e., oblique to bedding) appear uncommon in the sections from these deepest intervals.

Microfractures consistent with this pattern are found in a number of the remaining sections. One bedding plane microfracture that spans the width of the section (~6 cm) is present in a section from the shallowest depth (PX1-02). However, microfractures at oblique angles to bedding are also commonly found in the remaining sections. It is impossible to determine whether these oblique microcracks are part of a larger pattern.

3.2.3.3 COMPARISON WITH FRACTURE OBSERVATIONS FROM THE CORE DAMAGE STUDY

The foregoing observations closely parallel those presented by Holcomb et al. (in press) who examined 36 oriented thin sections prepared from six closely spaced cores drilled into the marker bed from a single room (Figure 2). Two boreholes were vertical, while four were inclined at 45° to vertical. Their specimens were not highly damaged and cracks appeared tensile or extensile in nature.

Microfractures in anhydrite predominated, were exclusively intergranular, and tended to be long and concentrated in narrow zones. Evidence for ligamentary bridging and frictional interlocking was common. Microfractures in anhydrite tended to closely follow the bedding plane laminations defined by the carbonate/clay/bitumen stringers. Microfractures in halite were rare and inevitably cleavage cracks. When microfractures in anhydrite approached halite grains, they often either terminated abruptly or diverted around the halite.

Fracture patterns reported by Holcomb et al. (1995) were likewise very similar to those found here. Long microfractures and microfracture zones in anhydrite, parallel to bedding, predominated. A

subordinate set of microfractures normal to bedding also occurred. Holcomb et al. also tentatively identified a third microfracture population, conjugate pairs inclined at roughly 45° to bedding, but evidence for this third set was weak. Holcomb et al. concluded that while the microfracture pattern was consistent with floor arching following room excavation, the microfractures probably occurred during coring: other geophysical evidence suggested that the microfractures were either not present or not open prior to core recovery.

Evidence for healed fractures in halite crystals was common (i.e., planar arrays of fluid inclusions and infilled cleavage cracks); however, Holcomb et al. observed no evidence for partial infilling of now-open microfractures. This observation was consistent with their conclusion that the dyed fractures were recent, and probably attributable to core recovery. This last observation differs from that of this study and possibly offers insight into the sequence of fracturing since the main difference between the earlier study and this one is the time of core recovery with respect to room excavation.

3.2.3.4 POSSIBLE SEQUENCE OF FRACTURE DEVELOPMENT

That some of the microfractures are either partially or completely infilled indicates that they must have been open *in situ* for an uncertain period of time prior to core recovery. Some extended period of time would be required to allow new fluids to percolate through the microfractures and precipitate minerals. Thus, except in those instances where the mineral infillings themselves have been fractured, recent coring can probably be discounted as the cause of microfracturing.

Given that the observed fracture patterns for both the completely and partially infilled microfractures are what would be expected from floor arching after room excavation (Borns and Stormont, 1989), it seems reasonable to conclude that much of the microfracturing dates either from that time or more recently. Similarly, the crack infilling observed here probably took place within the same time span. In instances where mineral infillings have subsequently been fractured again, two possibilities exist. Damage either occurred *in situ*, with both healing and continued floor arching taking place contemporaneously, during core recovery, or both. It is noted, however, that the observations here do not preclude the possibility that some or possibly all of the partially or completely infilled fractures may have existed *in situ* prior to excavation.

Time-series studies in and near the room where Holcomb et al. (1995) performed their investigation would provide an excellent opportunity to further elucidate the deformation and healing processes that occur in the marker bed following excavation, particularly since the initial conditions were thoroughly documented only ~1 year after room excavation.

4.0 RESULTS OF XRD AND MODAL ANALYSES

Mineralogies determined by the semiquantitative powder x-ray diffraction analyses are summarized in Table 6. The results in cases where two different samples were prepared from the same depth interval from the same core sample (but separated by up to several inches in the bedding plane) are summarized separately in Table 7. The results of the petrographic modal analyses are reported in Table 8. The grain size measurements which were performed simultaneously with the 300-point count modal analyses for cores E1X07 and E1X08 are summarized in Table 9.

4.1 Discussion of the Mineralogy of MB 139

The quantitative mineralogic studies performed on samples prepared from six large-diameter cores drilled into Marker Bed 139 from two different rooms at the WIPP repository reveal that although the marker bed is mineralogically complex, several general trends can nevertheless be identified.

The mineralogic data and whole-core observations (Appendix A) indicate that although the marker bed is laterally continuous, both the absolute vertical location and thickness of the marker bed vary significantly over lateral distances on the order of hundreds of feet. For example, E1X08 and E1X10 were drilled from the floor of Room E140 ~6 feet apart and both drill holes intersected the marker bed at a depth of ~3.5 feet. However, E1X07, which was drilled from the same room but about ~165 feet away from E1X08 and E1X10, did not intersect the marker bed for a full additional foot. Furthermore, whereas the marker bed is slightly over 2 feet in thickness at the E1X07 location, it is closer to 3 feet thick at the location of the E1X08, E1X10, and E1X11 cores. Similarly, when the differences in collar elevation (Table 1) are accounted for, P3X10 and P3X11, which were drilled from the floor of Room 3, indicate a variation in the absolute location of the upper contact of the marker bed of ~11 vertical feet compared with E1X08 and E1X10. On a more local scale, the undulatory nature of the upper contact, which is discussed in detail by Borns (1985), is evident in core E1X08 and is particularly conspicuous in core P3X10 (Appendix A).

With limited exceptions (see later discussion), the petrographic and powder diffraction (XRD) analyses for mineralogy are in good agreement. Anhydrite and halite are generally the most abundant minerals; however, polyhalite is a major and sometimes dominant mineral phase in the uppermost part of the marker bed. Finely crystalline carbonate is a consistent minor phase present throughout the marker bed that typically occurs in patches or wisps and constitutes up to several percent of the minerals present. The petrographic analyses consistently suggest somewhat higher amounts of carbonate than the XRD analyses (i.e., typically 5 to 10 volume percent versus trace to 5 weight percent); however, it is likely that the modal analyses are biased high due to the finely crystalline nature of this phase. The different petrographic analyses originally identified this phase as either magnesite or possibly dolomite (Table 8), although it is noted here that distinguishing these two phases using optical techniques is nearly impossible (e.g., Kerr, 1977). Nevertheless, in those cases where magnesite was identified optically, the powder x-ray diffraction analyses generally confirm the occurrence of magnesite (Table 6). Likewise, the XRD analyses confirm the occurrence of dolomite

Table 6. X-Ray Diffraction Analyses of MB 139 Core Samples

Core i.d.	Depth interval (feet)	Composition (wt %)				
		Anhydrite	Halite	Polyhalite	Carbonate	Other
E1X07	4.00-4.14	7	23	28	42†	trace§
	5.00-5.14	62	38	—	—	—
	5.73-5.87	81	19	—	—	—
E1X08	4.00-4.14	70	30	trace	—	—
	4.86-5.00	32	68	—	—	—
	5.71-5.85	98	2	—	—	—
E1X10	4.50	80	20	—	trace‡	trace¶
	5.00	73	26	—	1‡	trace¶
	5.25*	77	23	—	trace‡	trace¶★
	5.50	92	7	—	1‡	trace¶
	5.75*	94	4	—	2‡	trace¶
	6.25	96	trace	—	4‡	trace¶
E1X11	4.50	54	46	—	trace‡	trace¶
	4.75	68	32	—	tr‡	—
	5.00	66	30	—	4‡	trace¶
	5.25*	61	36	—	3‡	trace¶★
	5.75*	92	8	—	tr‡	trace¶
P3X10	5.15-5.39	47	52	—	1‡	—
	5.53-5.87*	50	44	5	1‡	—
P3X11	5.33-5.67*	12	7	80	1‡	—
	5.84-6.04	60	11	27	2‡	—
	6.88-7.22*	57	38	—	5‡	—
	7.55-7.72	72	28	—	—	—

* Average of two samples from the same depth interval but separated by a few inches in the bedding plane.

† ~30% was tentatively identified as ferroan dolomite or another cation-disordered Ca-Mg-Fe carbonate and ~12% was identified as aragonite. The occurrence of such a large quantity of carbonate is unusual and may indicate that the XRD sample prepared from this depth interval was not representative of the bulk material. Also, the contractor noted a high degree of uncertainty in the quantitative analysis for this sample since the optimal standards were not available for quantification.

‡ Magnesite.

§ Quartz was tentatively identified.

¶ Clay.

★ Gypsum.

Table 7. Comparison of XRD Analyses for Duplicate Samples*

Core i.d.	Depth interval (feet)	Composition (wt%)				
		Anhydrite	Halite	Polyhalite	Magnesite	Other
E1X10	5.25	56 99	44 1	— —	trace trace	trace† trace†‡
	5.75	93 97	4 3	— —	3 trace	trace† trace†
E1X11	5.25	54 69	44 28	— —	2 3	trace† trace†‡
	5.75	85 99	15 1	— —	trace trace	trace† —
P3X10	5.53-5.87	55 45	43 44	— 11	1 1	— —
P3X11	5.33-5.67	18 6	10 3	69 90	3 trace	— —
	6.88-7.22	55 58	39 37	— —	6 4	— —

* Samples were prepared from the same depth interval but spaced up to several inches apart in the bedding plane.
† Clay.
‡ Gypsum.

Table 8. Modal Analyses of MB 139 Core Samples

Core i.d.	Depth (feet)	Orient-ation*	Composition (vol %)				
			Anhydrite	Halite	Polyhalite	Carbonate†	Other
E1X07	4.00-4.14	H	50	44	5	1	—
		V	20	12	55	13	—
		V	27	14	57	3	—
	5.00-5.14	H	66	26	—	9	—
		V	79	18	—	3	—
		V	75	21	—	4	—
	5.73-5.87	H	82	17	—	trace	trace‡
		V	81	16	—	3	—
		V	92	4	—	4	—
E1X08	4.00-4.14	H	6	trace	87	5	1‡
		V	67	20	7	6	—
		V	33	2	56	7	1‡
	4.86-5.00	H	62	37	—	2	—
		V	48	51	—	2	—
		V	67	30	—	4	—
	5.71-5.85	H	80	3	—	16	—
		V	87	1	—	12	—
		V	86	2	—	10	1‡
E1X10	4.50	H	82	16	—	2	trace§
	5.00	H	72	26	—	2	trace§
	5.25	H	67	30	—	3	trace§
		V	99	1	—	trace	trace§
	5.50	H	93	2	—	5	trace§

Table 8. Modal Analyses of MB 139 Samples (Continued)

Core i.d.	Depth (feet)	Orient-ation*	Composition (vol %)				
			Anhydrite	Halite	Polyhalite	Carbonate†	Other
E1X10	5.75	H	95	—	—	5	—
		V	82	15	—	3	trace§
	6.25	V	100	—	—	trace	—
E1X11	4.50	H	60	37	—	3	trace§
	4.75	H	71	26	—	2	1§
	5.00	H	64	30	—	6	trace§
	5.25	H	69	26	—	5	trace§
		V	83	12	—	5	trace§
	5.75	H	44	56	—	trace	trace§
		V	100	—	—	trace	—
P3X10	5.15-5.39	H	68	25	—	4	4¶
		V	43	55	—	1	2¶
		V	58	37	—	3	2¶
P3X11	5.80-6.04	H	70	16	10	2	2¶
		V	46	13	31	9	1¶
		V	49	27	15	8	2¶
	7.55-7.72	H	96	1	1	1	trace¶
		V	90	9	—	—	1¶
		V	67	32	—	trace	1¶

* Orientation of section was either vertical (V) or horizontal in the plane of bedding (H).
† Very finely crystalline. Two contractors identified this phase as magnesite and one tentatively suggested the mineral dolomite. However, it is very difficult to distinguish magnesite and dolomite optically(e.g., Kerr, 1977) and both minerals are common in evaporitic assemblages (Adams et al., 1984).
‡ Pyrite.
§ Gypsum.
¶ Carbonaceous (bituminous) matter.

Table 9. Grain Size Distribution of Selected MB139 Core Samples

Core i.d.	Depth (feet)	Orientation*	Median		Sorting†
			ϕ‡	mm	ϕ‡
E1X07	4.00-4.14	H	2.94	0.130	1.91
		V	5.23	0.027	1.54
		V	4.69	0.040	1.33
	5.00-5.14	H	3.93	0.066	1.80
		V	4.45	0.046	2.02
		V	4.01	0.062	1.86
	5.73-5.87	H	5.79	0.018	1.51
		V	5.77	0.018	1.56
		V	5.91	0.017	1.02
E1X08	4.00-4.14	H	6.04	0.015	0.98
		V	5.34	0.025	2.00
		V	5.60	0.026	0.91
	4.86-5.00	H	3.89	0.067	2.06
		V	3.95	0.065	1.96
		V	4.65	0.040	2.15
	5.71-5.85	H	5.88	0.017	0.85
		V	6.14	0.014	0.83
		V	6.30	0.013	0.92

* Orientation of section was either vertical (V) or horizontal in the plane of bedding (H).

† Sorting as defined by Folk, 1980 (p. 42).

‡ Phi scale as defined by Blatt et al., 1972 (p. 46-47).

in at least one sample. The characteristic diffraction peaks for dolomite and magnesite are well separated and since both magnesite and dolomite are known accessory minerals in evaporitic rocks (e.g., Adams et al., 1984), it is possible that both minerals are present to a limited extent in the marker bed. Other phases which occasionally occur in trace amounts (<1%) include clay and gypsum.

The large discrepancies between the modal and XRD analyses which are apparent in some cases (Tables 6 and 8) are most likely attributable to the high heterogeneity exhibited by the marker bed on even the centimeter scale. In the cases where petrographic analyses were performed on three mutually perpendicular thin sections prepared from single samples, variations in the volumetric percentages of mineral phases of up to 30% are not uncommon (Table 8). This conclusion is also supported by the XRD results for duplicate samples prepared from the same depth interval (but spaced a few centimeters apart horizontally), which in some cases indicate substantially different bulk compositions (Table 7).

Based on his mesoscopic study of five cores obtained by drilling into the marker bed from the floor of Room 4 (Figure 2), Borns (1985) suggested that the marker bed could be divided into five zones: three visually distinct zones which comprised the bulk of the marker bed (II-IV), and upper (I) and lower (V) contact zones, both of which were only a few centimeters thick. Zone II was classified as massive polyhalitic anhydrite with stylolitic laminae, Zone III as mixed anhydrite and polyhalitic anhydrite with marbled texture, and Zone IV as laminated anhydrite with halite. The present study did not include analysis of samples extracted from either the upper or lower contact zones and hence there is no further discussion of the contact zones below.

The petrographic modal and XRD analyses and macroscopic observations (Appendix A) of the six cores studied here are to a large degree consistent with Borns's (1985) classification of the marker bed (note that macroscopic fracture descriptions were not provided for the cores studied here). However, access to cores from two additional areas of the facility underground (Figure 2), along with the quantitative laboratory mineralogic analyses, provide a substantially enlarged data base and thus the opportunity for modification.

In particular, the extent of the polyhalitic overprint characteristic of Zones II and III is shown to be highly variable. In the four cores taken from the E140 drift, Zone II is readily apparent in core E1X07 but not in the other cores (E1X08, E1X10, E1X11) which were taken ~165 feet away from E1X07. Similarly, for the cores taken from Room 3, Zone II is present in core P3X11, but appears absent in core P3X10. In those cores in which Zone II is apparent, the laboratory analyses indicate that halite is also present in significant amounts (~10 to 20%) and that polyhalite can comprise up to~60% of the minerals present. The occurrence of this phase is typically manifested by a distinctive salmon-pink color. Zone II is thus better characterized as polyhalitic anhydrite and halite, and, furthermore, only occasionally present. Zone III appears to be of very limited extent (~3 inches thick) in core E1X07 and lacking polyhalite. Although a polyhalitic overprint is well developed in the upper part of Zone III in core E1X08, it is absent from the lower part. Similarly, only one small band of polyhalitic anhydrite is apparent in Zone III in core E1X10, and none is apparent in Zone III in core E1X11. In the cores from Room 3, Zone III in P3X11 contains abundant polyhalite, but only

limited polyhalite in P3X11. Zone III in these cores is thus more accurately described as mixed anhydrite and halite with sporadic polyhalitic overprint, with halite accounting for 30 to 50% of the rock. Finally, Zone IV is well defined in all of the cores and characterized as mixed anhydrite and halite, although the bottom of this zone is nearly pure anhydrite. The main distinction between Zones III and IV is the transition from a marbled to laminated texture.

5.0 SUMMARY

As reported by Borns (1985) and earlier investigators cited by him, though Marker Bed 139 is areally extensive and continuous, it is internally complex and inhomogeneous -- both texturally and mineralogically, indicating a complex depositional and postdepositional history. This study offers further evidence for the internal complexity and inhomogeneity of the marker bed; however, comprehensive investigation of the diagenetic and geologic history of the marker bed is beyond the scope of this study. Instead, this study aimed to (1) quantify the mineral composition to support laboratory studies of hydrologic properties and facilitate correlation of transport properties with composition; (2) describe textures including grain size; and (3) describe observed porosity (Howarth, 1993).

Although many of the observations of this study are to a large degree consistent with Borns' (1985) classification of the marker bed derived from macroscopic observations of cores drilled from one room of the underground facility, the systematic petrographic study and quantitative laboratory analyses of six large-diameter cores from two additional areas of the underground facility have provided additional insight and the opportunity for further refinement. In particular, the studies carried out here indicate that Zone II is better characterized as polyhalitic anhydrite and halite, and, significantly, only occasionally present in the marker bed. Zone III is more accurately described as mixed anhydrite and halite with only a sporadic polyhalitic overprint, with halite accounting for 30 to 50% of the rock. Finally, Zone IV, which is well defined in all of the cores studied, is best characterized as mixed anhydrite and halite, with a gradual transition to nearly pure anhydrite at the base of the marker bed. The main distinction between Zones III and IV is a transition from marbled to laminated texture. Recently, *in situ* hydraulic fracturing tests (Beauheim et al., 1993b) have suggested that partially or fully healed fractures along these laminations are the preferred fluid flow pathways in the marker bed. The upper and lower contact zones (Zones I and V), neither of which is more than a few centimeters thick, were not studied here and so no revisions to Borns's classification are proposed.

The detailed petrographic and quantitative modal analyses further reveal that even within single zones of the marker bed, sudden transitions in mineralogy and/or texture occur even at the centimeter scale. Although the major mineralogic phases in the marker bed are anhydrite, halite, and polyhalite, these sudden transitions in mineralogy and/or texture are often marked by the occurrence of dark "stringers," which are fine laminations containing several minor phases, including carbonate, clay, and bituminous material.

Our observations also provide evidence for the existence of naturally occurring, localized zones of relatively higher porosity within the marker bed. It is unclear how connected this porosity is over large areas of the underground facility or what role it plays in the overall fluid transport properties of the marker bed. (It should be noted that this study did not include mesoscopic analysis of large-scale partings or fractures in the marker bed core samples). The above-mentioned "stringers" are one of the two microstructural features which are consistently associated with the small amount of porosity which is observed in the marker bed. Much of the porosity associated with the stringers

appears to reside in the carbonate phases. The other commonly observed form of porosity occurs as a penetrative microporosity which is again associated with minor phases, and specifically with small patches of finely crystalline carbonate which occur throughout the marker bed. The presence of blue dye in this microporosity is testimony to its interconnectedness throughout the bulk rock.

The only other porosity observed occurs in the form of discrete microfractures, some of which are again closely associated with the carbonate stringers and occur as bedding-plane parallel microfractures. The stringers, which have a stylolytic character, may themselves represent relict surfaces of fluid transport and dissolution, and the occurrence of microfractures along them suggests that they may be planes of weakness within the formation. The origin of many of the observed microfractures is unclear; however, the presence of partially and fully mineralized microcracks indicates that at least some of these microfractures are open in the marker bed as it exists *in situ*. The mineralized cracks also provide evidence that, at least under some circumstances, the marker bed may be capable of "healing" itself after disturbance.

6.0 REFERENCES

Adams, A.E., W.S. MacKenzie, and C. Guilford. 1984. *Atlas of Sedimentary Rocks Under the Microscope*. New York, NY: John Wiley and Sons.

Beauheim, R.L., R.M. Roberts, T.F. Dale, M.D. Fort, and W.A. Stensrud. 1993a. *Hydraulic Testing of Salado Formation Evaporites at the Waste Isolation Pilot Plant Site: Second Interpretive Report.* SAND92-0533. Albuquerque, NM: Sandia National Laboratories.

Beauheim, R.L., W.R. Wawersik, and R.M. Roberts. 1993b. "Coupled Permeability and Hydrofracture Tests to Assess the Waste-Containment Properties of Fractured Anhydrite," *International Journal of Rock Mechanics and Mining Sciences & Geomechanics Abstracts.* Vol. 30, no. 7, 1159-1163.

Blatt, H., G. Middleton, and R. Murray. 1972. *Origin of Sedimentary Rocks.* Englewood Cliffs, NJ: Prentice-Hall.

Borns, D.J. 1985. *Marker Bed 139: A Study of Drillcore from a Systematic Array.* SAND85-0023. Albuquerque, NM: Sandia National Laboratories.

Borns, D.J., and J.C. Stormont. 1989. "The Delineation of the Disturbed Rock Zone Surrounding Excavations in Salt," *Rock Mechanics as a Guide for Efficient Utilization of Natural Resources: Proceedings of the 30th U.S. Symposium on Rock Mechanics, Morgantown, WV, June 19-22, 1989.* Ed. A.W. Khair. Brookfield, VT: A.A. Balkema. 353-360.

Chung, F.H. 1974. "Quantitative Interpretation of X-ray Diffraction Patterns. II. Adiabatic Principle of X-ray Diffraction Analysis of Mixtures," *Journal of Applied Crystallography.* Vol. 7, pt. 6, 526-531.

Davies, P.B. 1991. *Evaluation of the Role of Threshold Pressure in Controlling Flow of Waste-Generated Gas into Bedded Salt at the Waste Isolation Pilot Plant.* SAND90-3246. Albuquerque, NM: Sandia National Laboratories.

Davies, P.B., L.H. Brush, M.A. Molecke, F.T. Mendenhall, and S.W. Webb, eds. 1991. *Waste-Generated Gas at the Waste Isolation Pilot Plant: Papers Presented at the Nuclear Energy Agency Workshop on Gas Generation and Release from Radioactive Waste Repositories.* SAND91-2378. Albuquerque, NM: Sandia National Laboratories.

Deer, W.A., R.A. Howie, and J. Zussman. 1966. *An Introduction to the Rock Forming Minerals.* London: Longman, Green, and Co., Ltd.

Folk, R. L. 1980. *Petrology of Sedimentary Rocks.* Austin, TX: Hemphill Publishing Co.

Freiman, S.W., and P.L. Swanson. 1990. "Fracture of Polycrystalline Ceramics," *Deformation Processes in Minerals, Ceramics, and Rocks.* Eds. D.J. Barber and P.G. Meredith. London: Unwin Hyman. 72-83.

Gonzales, M.M. 1989. *Compilation and Comparison of Test-Hole Location Surveys in the Vicinity of the Waste Isolation Pilot Plant Site.* SAND88-1065. Albuquerque, NM: Sandia National Laboratories.

Holcomb, D.J., D.H. Zeuch, K. Morin, R. Hardy, and T.V. Tormey. 1995. *Field and Laboratory Investigations of Coring-Induced Damage in Core Recovered from Marker Bed 139 at the WIPP Underground Facility.* SAND94-2757. Albuquerque, NM: Sandia National Laboratories.

Howarth, S.M. 1993. *Conceptual Plan: Two-Phase Flow Laboratory Program for the Waste Isolation Pilot Plant.* SAND93-1197. Albuquerque, NM: Sandia National Laboratories.

Howarth, S.M. 1994. "Test Plan: Two-Phase Flow Laboratory Program for the Waste Isolation Pilot Plant." Albuquerque, NM: Sandia National Laboratories.

Jenkins, R., ed. 1986. *Methods and Practices in X-Ray Diffraction.* Swarthmore, PA: JCPDS—International Centre for Diffraction Data.

Kerr, P.F. 1977. *Optical Mineralogy.* 4th ed. New York, NY: McGraw-Hill.

Lowenstein, T. 1982. "Primary Features in a Potash Evaporite Deposit, the Permian Salado Formation of West Texas and New Mexico," *Depositional and Diagenetic Spectra of Evaporites - A Core Workshop, Calgary, Alberta, Canada, June 26-27, 1982.* Eds. C.R. Handford, R.G. Loucks, and G.R. Davies. SEPM Core Workshop No. 3. [Calgary: Society of Economic Paleontologists and Mineralogists]. 276-304.

Moore, D.M., and R.C. Reynolds, Jr. 1989. *X-Ray Diffraction and the Identification and Analysis of Clay Minerals.* New York, NY: Oxford University Press.

7.0 APPENDIX A

Photographs of whole cores E1X07, E1X08, E1X10, E1X11, P3X10, AND P3X11.

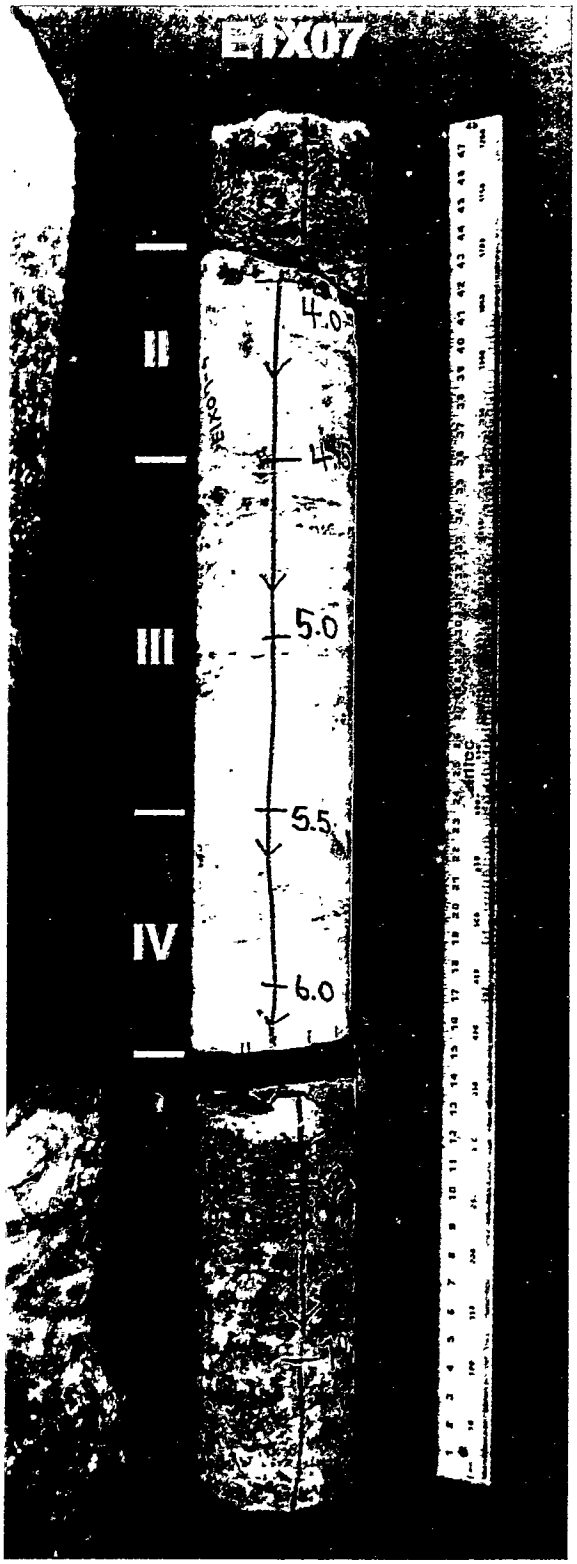
E1X07
II
III
IV
4.0
5.0
5.5
6.0

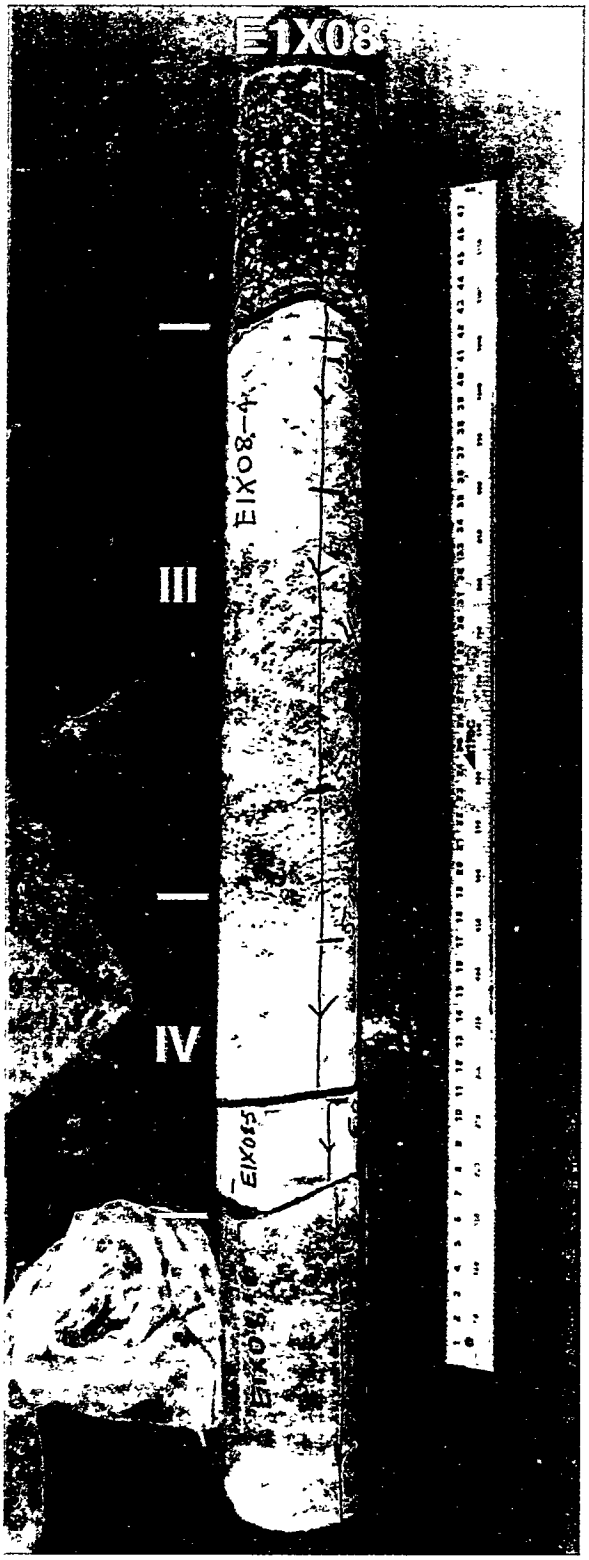
E1X08
III
IV
E1X08-4
E1X08-5

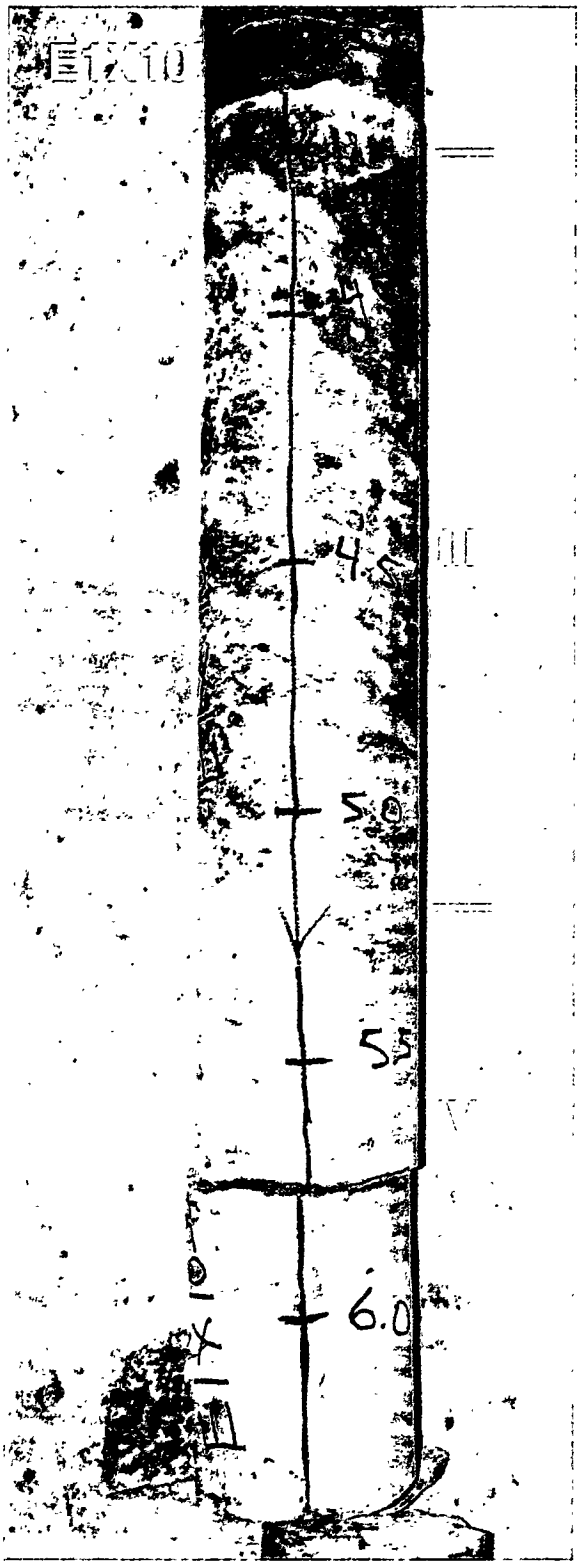
E1X10
4.5
5.0
5.5
6.0

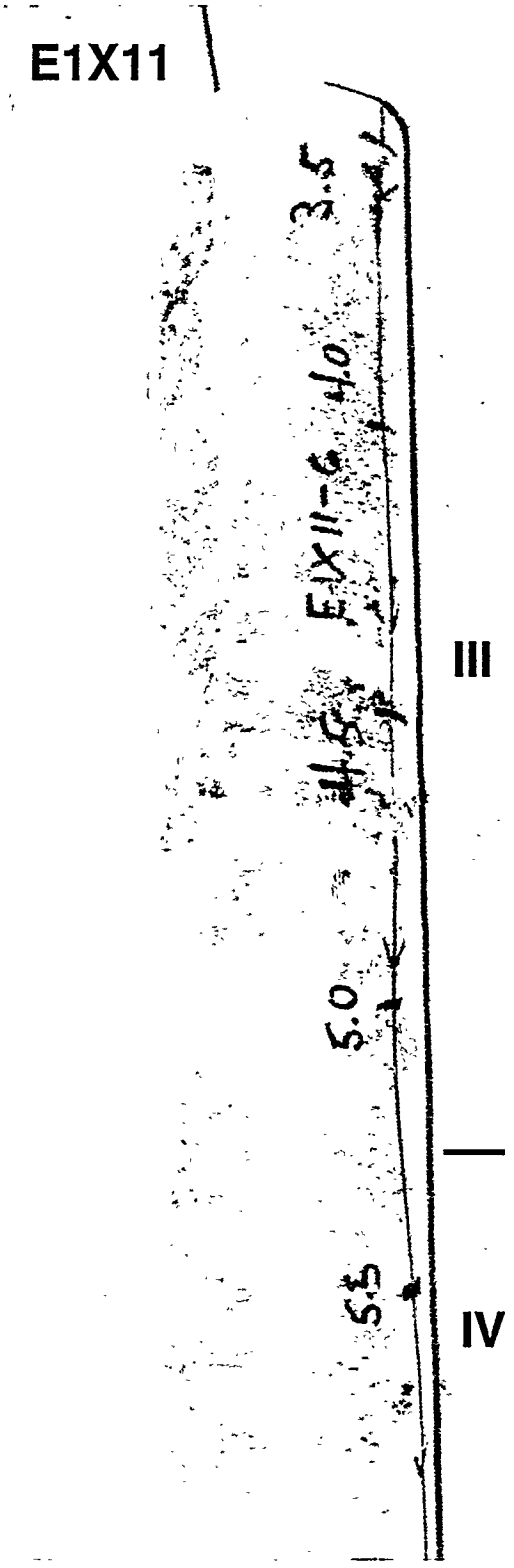
E1X11
3.5
4.0
E1X11-6
4.5
5.0
5.5
III
IV

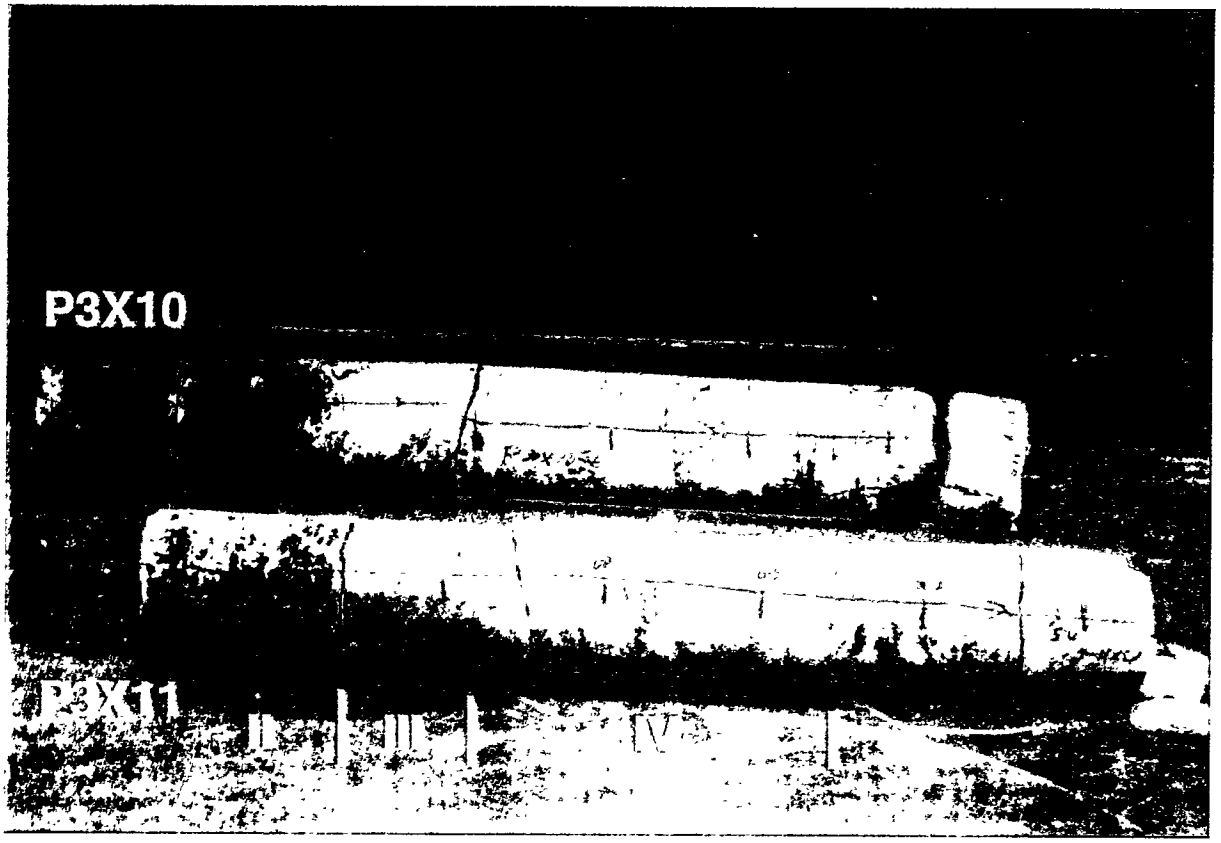
P3X10

WIPP
UC721 - DISTRIBUTION LIST

Federal Agencies

US Department of Energy (6)
Office of Civilian Radioactive Waste Mgmt.
Attn: Deputy Director, RW-2
Associate Director, RW-10/50
Office of Prog. & Resources Mgmt.
Office of Contract Business Mgmt.
Director, RW-22
Analysis & Verification Division
Associate Director, RW-30
Office of Systems & Compliance
Associate Director, RW-40
Office of Storage & Transportation
Director, RW-4/5
Office of Strategic Planning and International Programs
Office of External Relations
Forrestal Building
Washington, DC 20585

US Department of Energy
Albuquerque Operations Office
Attn: National Atomic Museum Library
P.O. Box 5400
Albuquerque, NM 87185-5400

US Department of Energy
Research & Waste Management Division
Attn: Director
P.O. Box E
Oak Ridge, TN 37831

US Department of Energy (5)
Carlsbad Area Office
Attn: G. Dials
D. Galbraith
M. McFadden
R. Lark
J. A. Mewhinney
P.O. Box 3090
Carlsbad, NM 88221-3090

US Department of Energy
Office of Environmental Restoration and Waste Management
Attn: J. Lytle, EM-30
Forrestal Building
Washington, DC 20585-0002

US Department of Energy (3)
Office of Environmental Restoration and Waste Management
Attn: M. Frei, EM-34, Trevion II
Washington, DC 20585-0002

US Department of Energy
Office of Environmental Restoration and Waste Management
Attn: S. Schneider, EM-342, Trevion II
Washington, DC 20585-0002

US Department of Energy (2)
Office of Environment, Safety & Health
Attn: C. Borgstrom, EH-25
R. Pelletier, EH-231
Washington, DC 20585

US Department of Energy (2)
Idaho Operations Office
Fuel Processing & Waste Mgmt. Division
785 DOE Place
Idaho Falls, ID 83402

US Environmental Protection Agency (2)
Radiation Protection Programs
Attn: M. Oge
ANR-460
Washington, DC 20460

Boards

Defense Nuclear Facilities Safety Board
Attn: D. Winters
625 Indiana Ave. NW, Suite 700
Washington, DC 20004

Nuclear Waste Technical Review Board (2)
Attn: Chairman
S. J. S. Parry
1100 Wilson Blvd., Suite 910
Arlington, VA 22209-2297

State Agencies

Attorney General of New Mexico
P.O. Drawer 1508
Santa Fe, NM 87504-1508

Environmental Evaluation Group (3)
Attn: Library
7007 Wyoming NE
Suite F-2
Albuquerque, NM 87109

NM Energy, Minerals, and Natural
Resources Department
Attn: Library
2040 S. Pacheco
Santa Fe, NM 87505

NM Environment Department (3)
Secretary of the Environment
Attn: Mark Weidler
1190 St. Francis Drive
Santa Fe, NM 87503-0968

NM Bureau of Mines & Mineral Resources
Socorro, NM 87801

NM Environment Department
WIPP Project Site
Attn: P. McCasland
P.O. Box 3090
Carlsbad, NM 88221

Laboratories/Corporations

Battelle Pacific Northwest Laboratories
Attn: R. E. Westerman, MSIN P8-44
Battelle Blvd.
Richland, WA 99352

INTERA, Inc.
Attn: G. A. Freeze
1650 University Blvd. NE, Suite 300
Albuquerque, NM 87102

INTERA, Inc.
Attn: J. F. Pickens
6850 Austin Center Blvd., Suite 300
Austin, TX 78731

INTERA, Inc.
Attn: W. Stensrud
P.O. Box 2123
Carlsbad, NM 88221

Los Alamos National Laboratory
Attn: B. Erdal, INC-12
P.O. Box 1663
Los Alamos, NM 87544

RE/SPEC, Inc
Attn: Angus Robb
4775 Indian School NE, Suite 300
Albuquerque, NM 87110-3927

RE/SPEC, Inc
Attn: J. L. Ratigan
P.O. Box 725
Rapid City, SD 57709

Tech Reps, Inc. (3)
Attn: J. Chapman (1)
Loretta Robledo (2)
5000 Marble NE, Suite 222
Albuquerque, NM 87110

Westinghouse Electric Corporation (5)
Attn: Library
J. Epstein
J. Lee
B. A. Howard
R. Kehrman
P.O. Box 2078
Carlsbad, NM 88221

S. Cohen & Associates
Attn: Bill Thurber
1355 Beverly Road
McLean, VA 22101

Rock Physics Associates
Attn: J. Walls
4320 Stevens Creek Blvd., Suite 282
San Jose, CA 95129

TerraTek, Inc.
Attn: J. McLennan
P.O. Box 8275
Salt Lake City, UT 84108-8275

**National Academy of Sciences,
WIPP Panel**

Howard Adler
Oxyrase, Incorporated
7327 Oak Ridge Highway
Knoxville, TN 37931

Bob Andrews
Board of Radioactive Waste Management
GF456
2101 Constitution Ave.
Washington, DC 20418

Rodney C. Ewing
Department of Geology
University of New Mexico
Albuquerque, NM 87131

Charles Fairhurst
Department of Civil and Mineral Engineering
University of Minnesota
500 Pillsbury Dr. SE
Minneapolis, MN 55455-0220

B. John Garrick
PLG Incorporated
4590 MacArthur Blvd., Suite 400
Newport Beach, CA 92660-2027

Leonard F. Konikow
US Geological Survey
431 National Center
Reston, VA 22092

Carl A. Anderson, Director
Board of Radioactive Waste Management
National Research Council
HA 456
2101 Constitution Ave. NW
Washington, DC 20418

Christopher G. Whipple
ICF Kaiser Engineers
1800 Harrison St., 7th Floor
Oakland, CA 94612-3430

John O. Blomeke
720 Clubhouse Way
Knoxville, TN 37909

Sue B. Clark
University of Georgia
Savannah River Ecology Lab
P.O. Drawer E
Aiken, SC 29802

Konrad B. Krauskopf
Department of Geology
Stanford University
Stanford, CA 94305-2115

Della Roy
Pennsylvania State University
217 Materials Research Lab
Hastings Road
University Park, PA 16802

David A. Waite
CH_2 M Hill
P.O. Box 91500
Bellevue, WA 98009-2050

Thomas A. Zordon
Zordan Associates, Inc.
3807 Edinburg Drive
Murrysville, PA 15668

Universities

University of New Mexico
Geology Department
Attn: Library
141 Northrop Hall
Albuquerque, NM 87131

University of Washington
College of Ocean & Fishery Sciences
Attn: G. R. Heath
583 Henderson Hall, HN-15
Seattle, WA 98195

Libraries

Thomas Brannigan Library
Attn: D. Dresp
106 W. Hadley St.
Las Cruces, NM 88001

Government Publications Department
Zimmerman Library
University of New Mexico
Albuquerque, NM 87131

New Mexico Junior College
Pannell Library
Attn: R. Hill
Lovington Highway
Hobbs, NM 88240

New Mexico State Library
Attn: N. McCallan
325 Don Gaspar
Santa Fe, NM 87503

New Mexico Tech
Martin Speere Memorial Library
Campus Street
Socorro, NM 87810

WIPP Public Reading Room
Carlsbad Public Library
101 S. Halagueno St.
Carlsbad, NM 88220

Foreign Addresses

Atomic Energy of Canada, Ltd.
Whiteshell Laboratories
Attn: B. Goodwin
Pinawa, Manitoba, CANADA R0E 1L0

Francois Chenevier (2)
ANDRA
Route de Panorama Robert Schumann
B. P. 38
92266 Fontenay-aux-Roses, Cedex
FRANCE

Claude Sombret
Centre d'Etudes Nucleaires de la Vallee Rhone
CEN/VALRHO
S.D.H.A. B.P. 171
30205 Bagnols-Sur-Ceze, FRANCE

Commissariat a L'Energie Atomique
Attn: D. Alexandre
Centre d'Etudes de Cadarache
13108 Saint Paul Lez Durance Cedex
FRANCE

Bundesanstalt fur Geowissenschaften und
Rohstoffe
Attn: M. Langer
Postfach 510 153
D-30631 Hannover, GERMANY

Bundesministerium fur Forschung und
Technologie
Postfach 200 706
5300 Bonn 2, GERMANY

Institut fur Tieflagerung
Attn: K. Kuhn
Theodor-Heuss-Strasse 4
D-3300 Braunschweig, GERMANY

Gesellschaft fur Anlagen und Reaktorsicherheit
(GRS)
Attn: B. Baltes
Schwertnergasse 1
D-50667 Cologne, GERMANY

Shingo Tashiro
Japan Atomic Energy Research Institute
Tokai-Mura, Ibaraki-Ken, 319-11
JAPAN

Netherlands Energy Research Foundation ECN
Attn: J. Prij
3 Westerduinweg
P.O. Box 1
1755 ZG Petten
THE NETHERLANDS

Svensk Karnbransleforsorjning AB
Attn: F. Karlsson
Project KBS (Karnbranslesakerhet)
Box 5864
S-102 48 Stockholm
SWEDEN

Nationale Genossenschaft fur die Lagerung
Radioaktiver Abfalle (2)
Attn: S. Vomvoris
P. Zuidema
Hardstrasse 73
CH-5430 Wettingen
SWITZERLAND

AEA Technology
Attn: J. H. Rees
D5W/29 Culham Laboratory
Abington, Oxfordshire OX14 3DB
UNITED KINGDOM

AEA Technology
Attn: W. R. Rodwell
044/A31 Winfrith Technical Centre
Dorchester, Dorset DT2 8DH
UNITED KINGDOM

AEA Technology
Attn: J. E. Tinson
B4244 Harwell Laboratory
Didcot, Oxfordshire OX11 ORA
UNITED KINGDOM

Internal

MS	Org.	
0750	6116	D. J. Borns
0751	6117	J. T. Fredrich (10)
0751	6117	D. J. Holcomb
0751	6117	W. R. Wawersik
0751	6117	D. H. Zeuch (5)

0751	6117	File
1320	6719	E. J. Nowak
1322	6121	J. R. Tillerson
1324	6115	P. B. Davies
1324	6115	S. M. Howarth (15)
1325	6313	N. S. Brodsky
1328	6749	D. R. Anderson
1328	6741	H. N. Jow
1335	6705	M. Chu
1341	6811	A. L. Stevens
1341	6748	J. T. Holmes
1395	6700	P. Brewer
1395	6800	L. Shephard
1395	6707	M. Marietta
1395	6841	V. H. Slaboszewicz

1330	6752	C. B. Michaels (2)
1330	6752	NWM Library (20)
9018	8523-2	Central Technical Files
0899	4414	Technical Library (5)
0619	12615	Print Media
0100	7613-2	Document Processing (2) for DOE/OSTI